High-Fidelity Simulations of Complex High-Speed Flows

Dr. Ali Uzun

Senior Research Scientist

National Institute of Aerospace

ali.uzun@nasa.gov

NASA Langley Computational AeroSciences Branch

Building 1268, Room 1040

September 15, 2015

Introduction

- High-fidelity numerical simulations have been performed in a number of past/current projects:
  - Aeroacoustics of subsonic jets
  - Resonance-enhanced micro-actuators that generate pulsed micro-jets for flow control
  - Supersonic impinging jets (STOVL aircraft)
  - Boundary layer transition delay via discrete roughness elements
  - Separated flows
- Complex high-speed flow phenomena
- Physical experiments are useful but provide limited amount of information
- Numerical simulations provide much more detailed information that help towards a better understanding of complex flow physics

Numerical Methods for High-Fidelity Flow Solver

- Discretized compressible Navier-Stokes equations in generalized curvilinear coordinates
- High-order compact finite difference schemes
- High-order spatial filtering for numerical stability
- Explicit and implicit time advancement schemes
- Multi-block and overset grid capability to handle complex geometry
- Parallelization based on domain-decomposition
- Artificial dissipation for shock-capturing
- Can be run in Direct Numerical Simulation (DNS) and Large Eddy Simulation (LES) modes
- Methodology in development for over a decade

General Form of a Compact Finite Difference Equation for the First Derivative

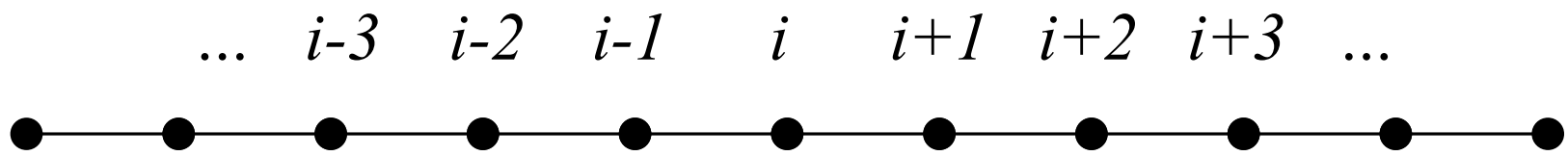

$$\beta f'_{i-2} + \alpha f'_{i-i} + f'_i + \alpha f'_{i+1} + \beta f'_{i+2} =$$

$$a\frac{f_{i+1} - f_{i-1}}{2\Delta x} + b\frac{f_{i+2} - f_{i-2}}{4\Delta x} + c\frac{f_{i+3} - f_{i-3}}{6\Delta x}$$

- **Relationships among the coefficients in the above equation are established by matching of the coefficients obtained by the substitution of Taylor series expansions**

Compact Finite Difference Schemes

- **Following constraints need to be satisfied for the desired order of accuracy:**
- **Second-order:** $1 + 2\alpha + 2\beta = a + b + c$
- **Fourth-order:** $2\frac{3!}{2!}(\alpha + 2^2\beta) = a + 2^2 b + 3^2 c$
- **Sixth-order:** $2\frac{5!}{4!}(\alpha + 2^4\beta) = a + 2^4 b + 3^4 c$
- **Eighth-order:** $2\frac{7!}{6!}(\alpha + 2^6\beta) = a + 2^6 b + 3^6 c$
- **Tenth-order:** $2\frac{9!}{8!}(\alpha + 2^8\beta) = a + 2^8 b + 3^8 c$
- **Various schemes can be derived based on above constraints**
- **Setting** $\alpha = \beta = 0$ **yields explicit schemes**
- **Tri-diagonal sixth-order scheme with a 5-point RHS stencil (**$\beta = 0$**,** $c = 0$**,** $\alpha = 1/3$**) is popular**

Implicit Time Advancement

- **Unfactored algorithm:**

$$\left[\mathbf{I} + h(\delta_\xi \hat{\mathbf{A}}^m + \delta_\eta \hat{\mathbf{B}}^m + \delta_\zeta \hat{\mathbf{C}}^m)\right] \Delta\hat{\mathbf{Q}}^m = \mathbf{R}^m$$

- **Approximately-factored algorithm:**

$$\left[\mathbf{I} + h\delta_\xi \hat{\mathbf{A}}^m\right] \left[\mathbf{I} + h\delta_\eta \hat{\mathbf{B}}^m\right] \left[\mathbf{I} + h\delta_\zeta \hat{\mathbf{C}}^m\right] \Delta\hat{\mathbf{Q}}^m = \mathbf{R}^m$$

where m is the sub-iteration index, $h = 2\Delta t/3$,

$$\mathbf{R}^m = -h\left[\delta_\xi \hat{\mathbf{F}}^m + \delta_\eta \hat{\mathbf{G}}^m + \delta_\zeta \hat{\mathbf{H}}^m\right] - \frac{(3\hat{\mathbf{Q}}^m - 4\hat{\mathbf{Q}}^n + \hat{\mathbf{Q}}^{n-1})}{3}$$

$$\hat{\mathbf{A}} = \frac{\partial \hat{\mathbf{F}}}{\partial \hat{\mathbf{Q}}},\ \hat{\mathbf{B}} = \frac{\partial \hat{\mathbf{G}}}{\partial \hat{\mathbf{Q}}},\ \hat{\mathbf{C}} = \frac{\partial \hat{\mathbf{H}}}{\partial \hat{\mathbf{Q}}},\ \delta_\xi = \frac{\partial}{\partial \xi},\ \delta_\eta = \frac{\partial}{\partial \eta},\ \delta_\zeta = \frac{\partial}{\partial \zeta}$$

Implicit Time Advancement

- **Approximately-factored form can be solved as:**

$$\textbf{first sweep:} \quad \left[\mathbf{I} + h\delta_\xi \hat{\mathbf{A}}^m\right] (\Delta\mathbf{Q}^*)^m = \mathbf{R}^m$$

$$\textbf{second sweep:} \quad \left[\mathbf{I} + h\delta_\eta \hat{\mathbf{B}}^m\right] (\Delta\mathbf{Q}')^m = (\Delta\mathbf{Q}^*)^m$$

$$\textbf{third sweep:} \quad \left[\mathbf{I} + h\delta_\zeta \hat{\mathbf{C}}^m\right] \Delta\hat{\mathbf{Q}}^m = (\Delta\mathbf{Q}')^m$$

- **Note that** $\hat{\mathbf{Q}}^{m+1} = \hat{\mathbf{Q}}^m + \Delta\hat{\mathbf{Q}}^m$
- **Iteration is continued until convergence**
- **This procedure forms the basis of the alternating-direction-implicit (ADI) time advancement scheme**
- **For example: for CFL = 25, usually three sub-iterations are needed for the initial residual to drop by two orders of magnitude**

Code Parallelization Strategy

- **The domain is divided into many sub-blocks**

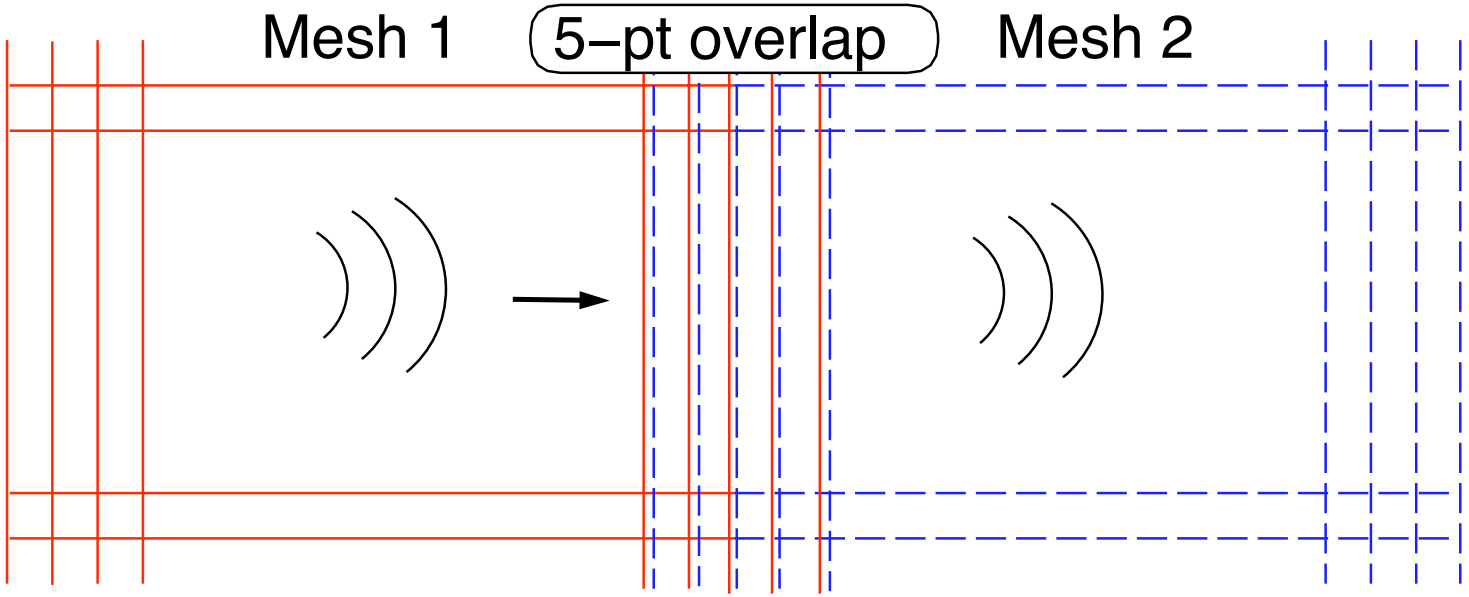

- **High-order schemes involve scalar/block tri-diagonal systems with a centered RHS stencil**
- **Centered schemes are applied away from overlap boundary**
- **One-sided or biased computational stencils are used near overlap boundary**

Code Parallelization Strategy

- **Data exchange is needed in the overlap region**

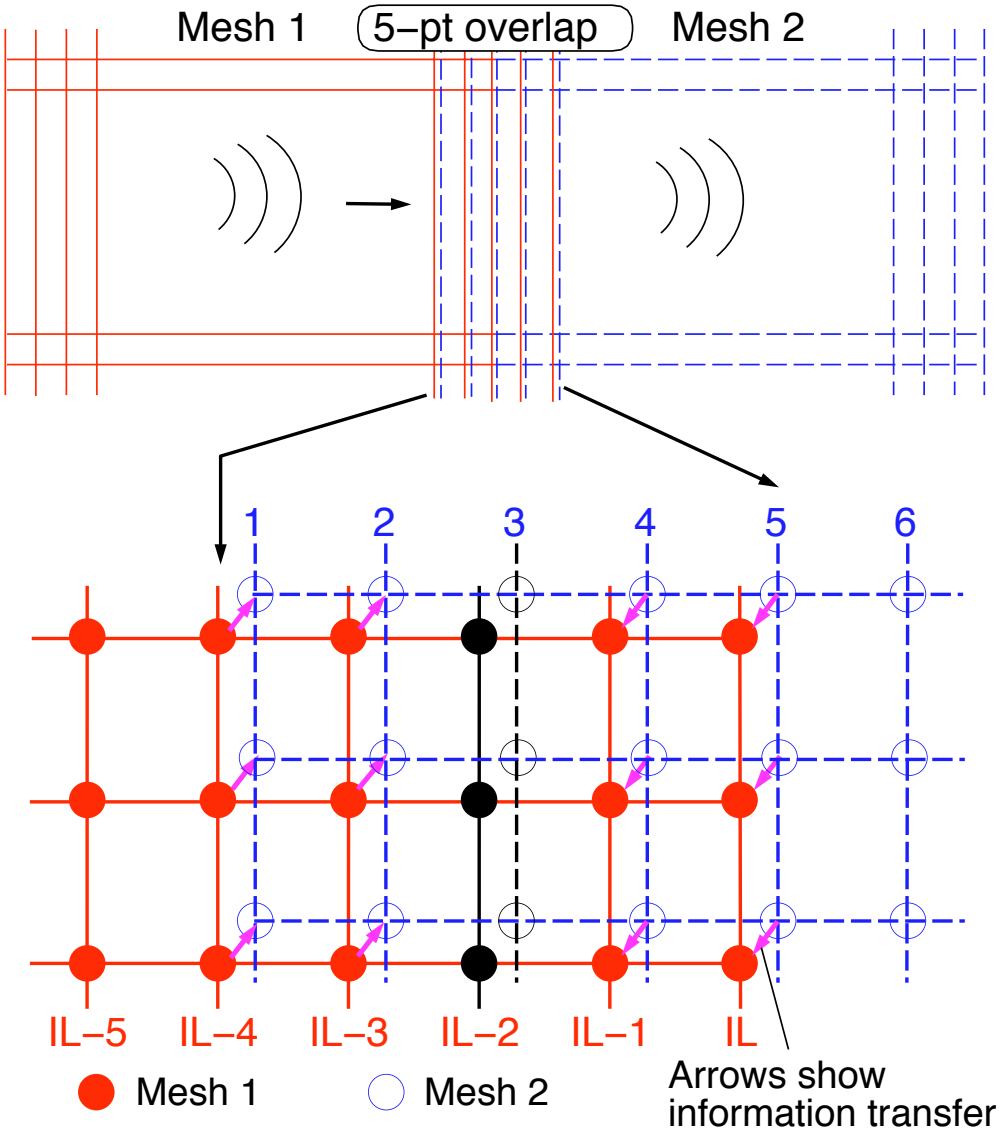

Parallel Speedup on IBM Blue Gene/Q (Fixed Total Problem Size)

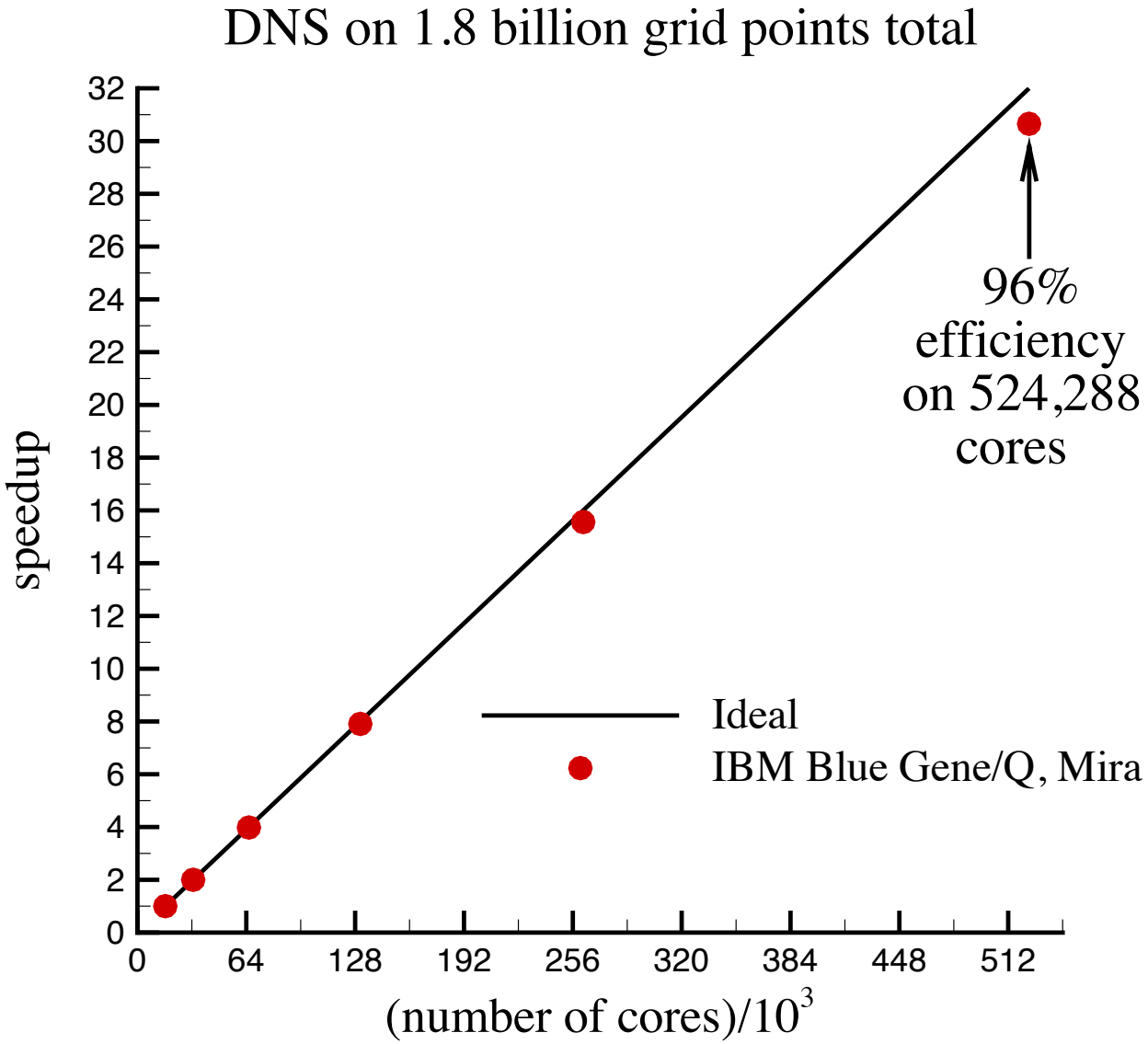

Some Applications of Simulation Methodology

Jet Engine Noise Problem

- Much of the noise of a jet engine is the aerodynamic noise generated by the high-speed jet exhaust flow
- Noise is a by-product of flow mixing and turbulence
- Significant amount of ongoing research on jet noise reduction technologies
- A promising jet noise reduction technology is the so-called “chevron nozzle”
- Chevron nozzles normally reduce the low-frequency noise at the expense of elevated high-frequency noise

Chevron Nozzles

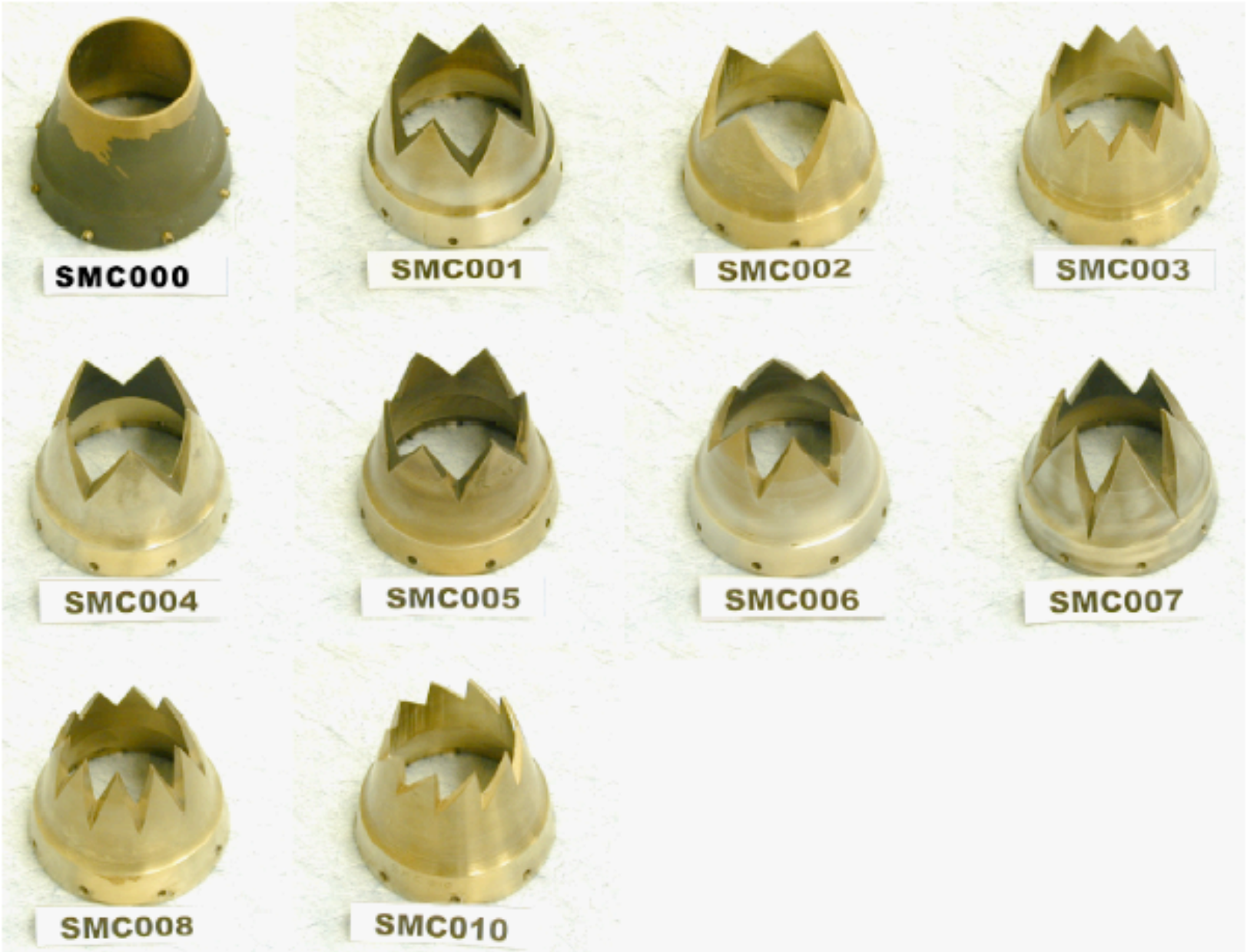

Chevron Nozzles

- **Chevrons generate axial vorticity which introduces mean flow inhomogeneity in azimuthal direction**
- **Jet mean flow comparison at $x/D = 0.5$:**

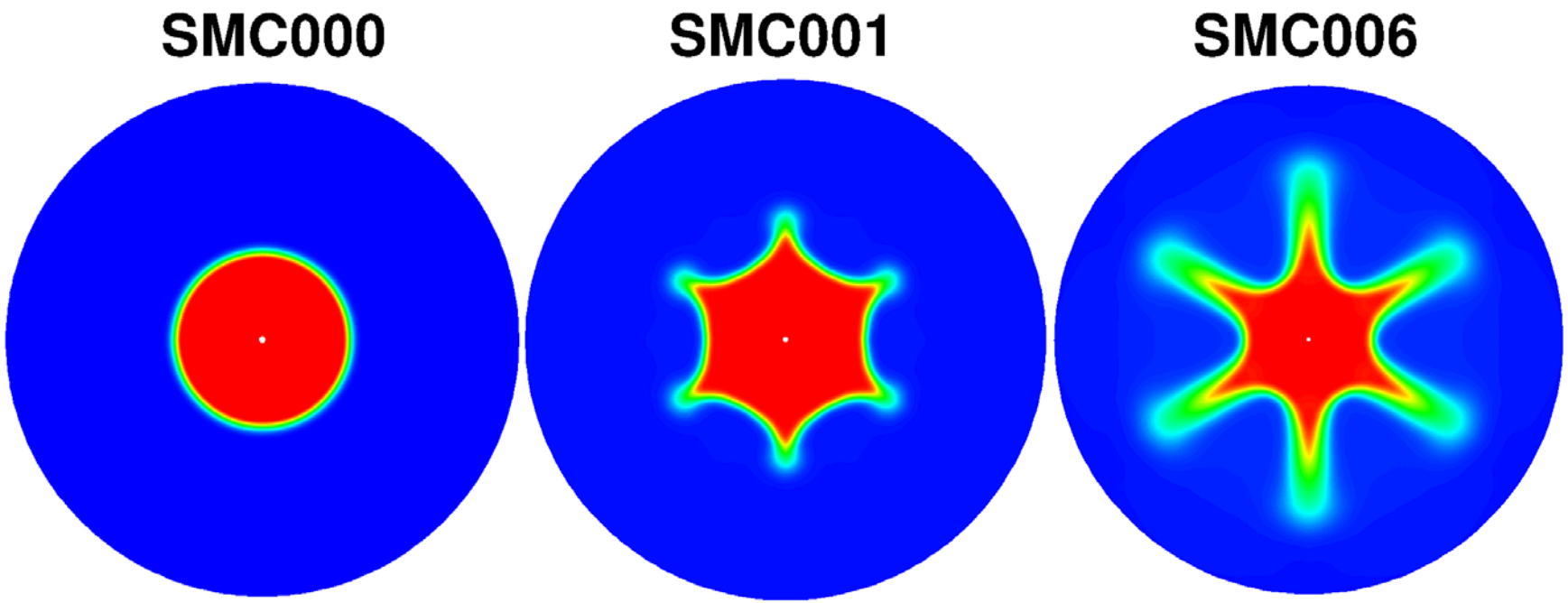

Why are Chevrons Effective in Low-Frequency Noise Reduction?

- **Hydrodynamic stability analysis shows that the azimuthal mean-flow inhomogenity causes:**
  - **Reduction in growth rate and convection speeds of dominant instability waves**
  - **Reduction in hydrodynamic near-field pressure fluctuations generated by dominant instability waves**
- **See the following paper for more details:**

  A. Uzun, F. Alvi, T. Colonius and M. Y. Hussaini, "Spatial Stability Analysis of Subsonic Jets Modified for Low-Frequency Noise Reduction," AIAA Journal, August 2015.

SMC006 Chevron Nozzle Surface Grid

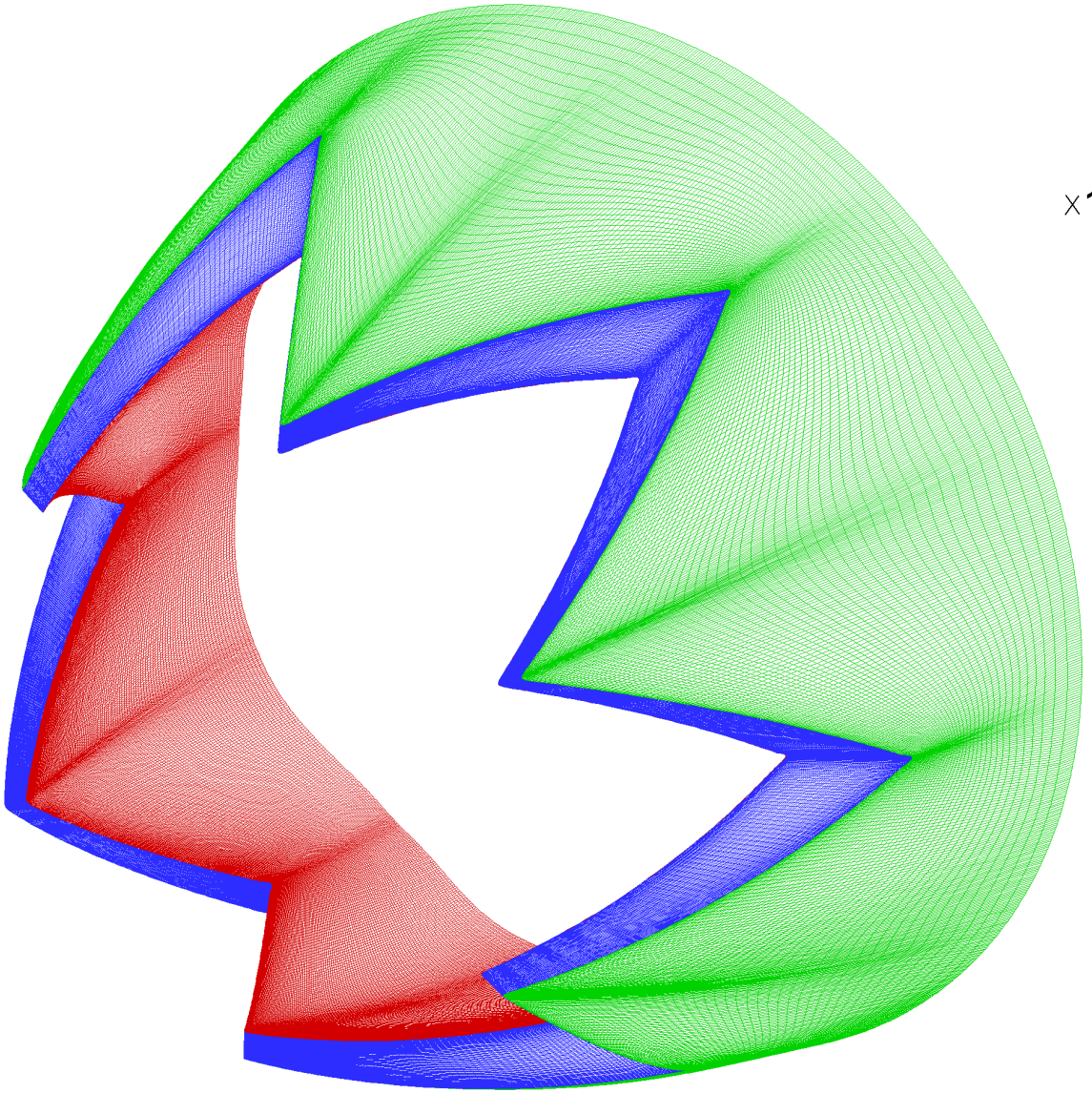

Grid Transition in Near-Nozzle Region

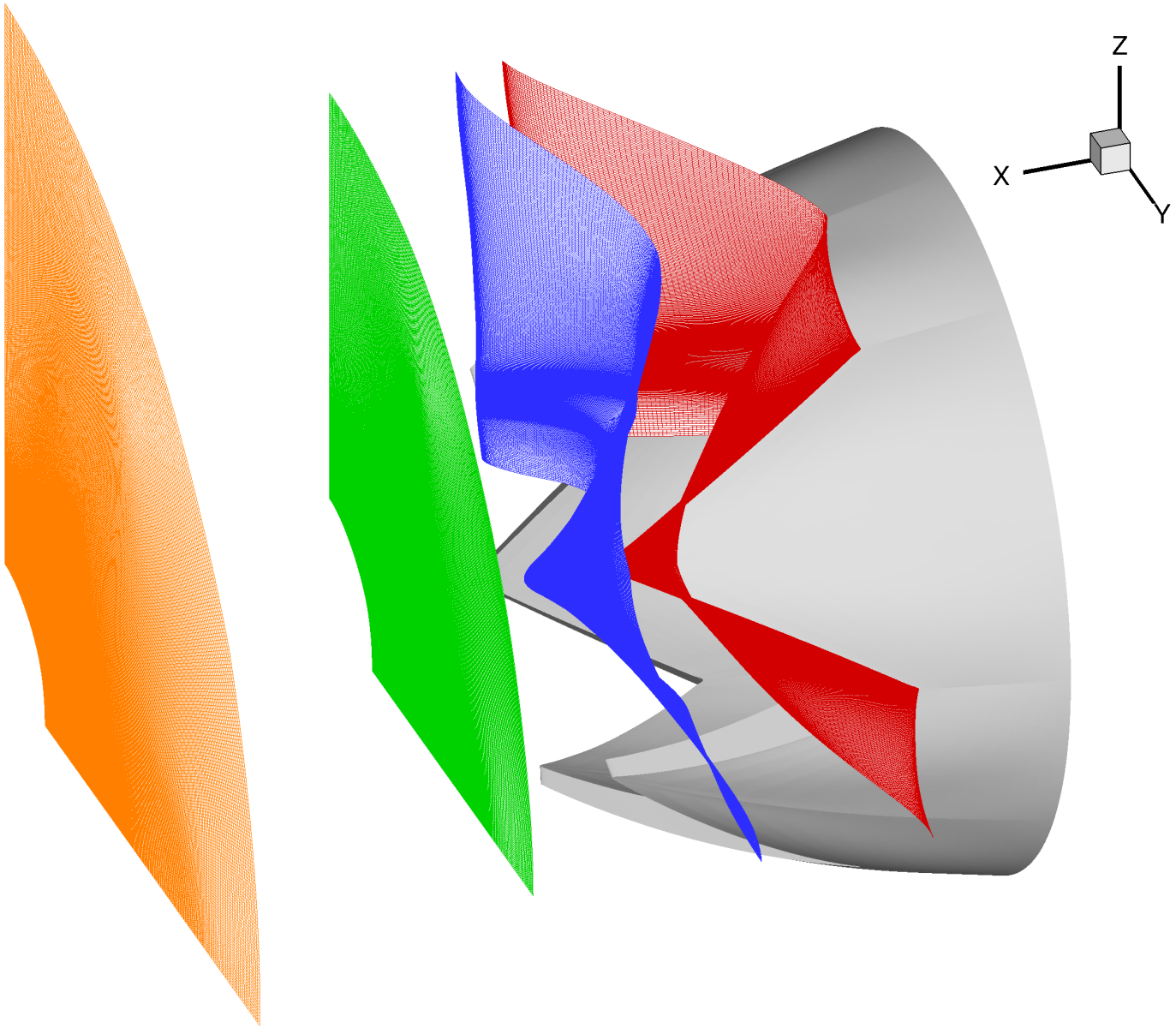

Overset Grids to Avoid Centerline Singularity

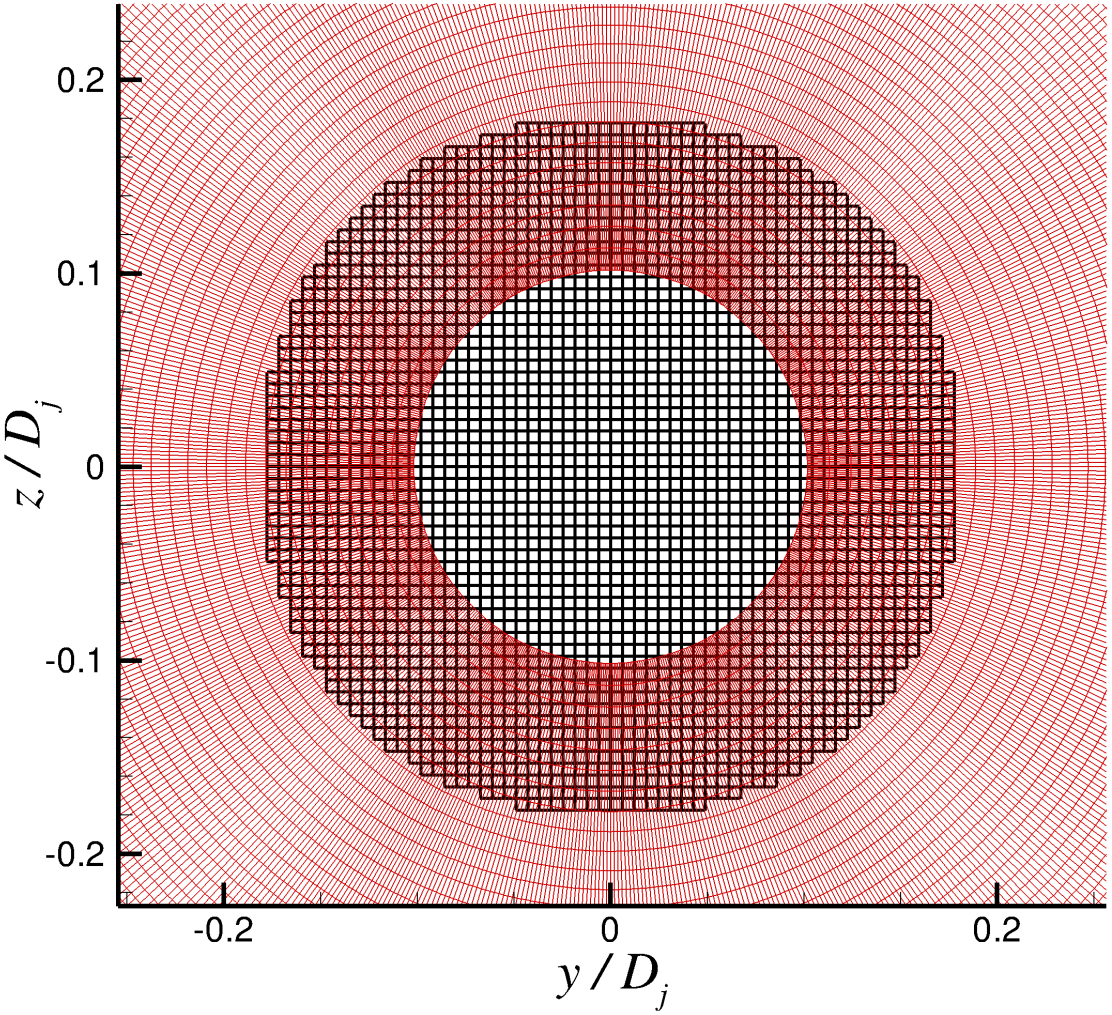

SMC006 Chevron Jet Simulations

- **Mach 0.9 unheated jet exhausting from SMC006 chevron nozzle geometry**
- **Axial domain size is set to $30D_j$ in simulation**
- **500 million grid points total**
- **The first $10D_j$ of domain has 400 million points**
- **Estimated experimental Reynolds number is about 1.2 million**
- **Simulations were performed at two different Reynolds numbers:**
  - **$Re_D = 100,000$ (with implicit SGS model)**
  - **$Re_D = 1,000,000$ (with Vreman's SGS model)**
- **We include a pipe upstream of nozzle inlet and employ a special procedure to generate turbulent boundary layers for nozzle inflow**

Instantaneous Jet Flow Field Visualization

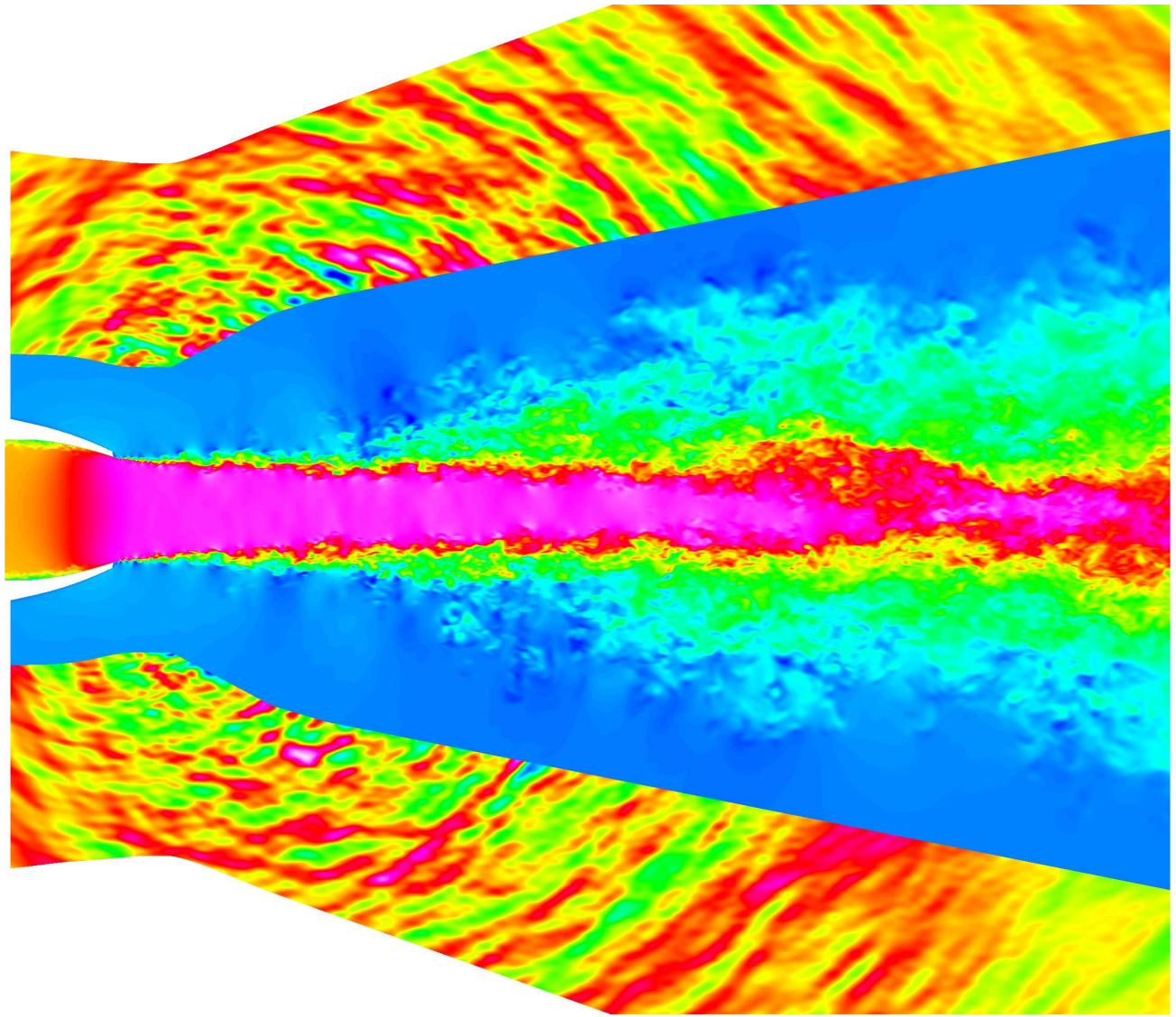

Axial Velocity Contours at $x/D_j = 2$

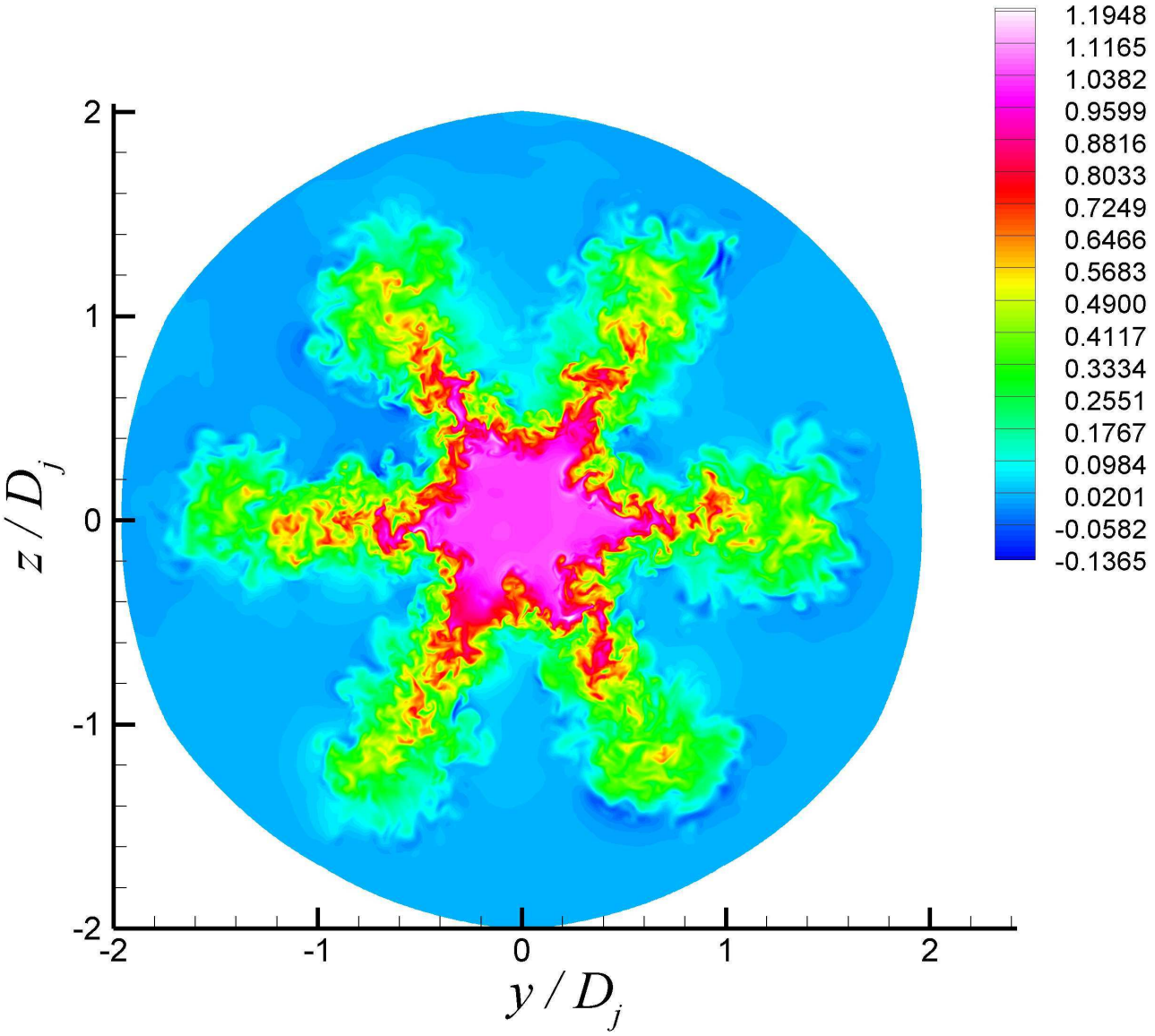

One-Third Octave Noise Spectra Comparison at 90° from Jet Axis

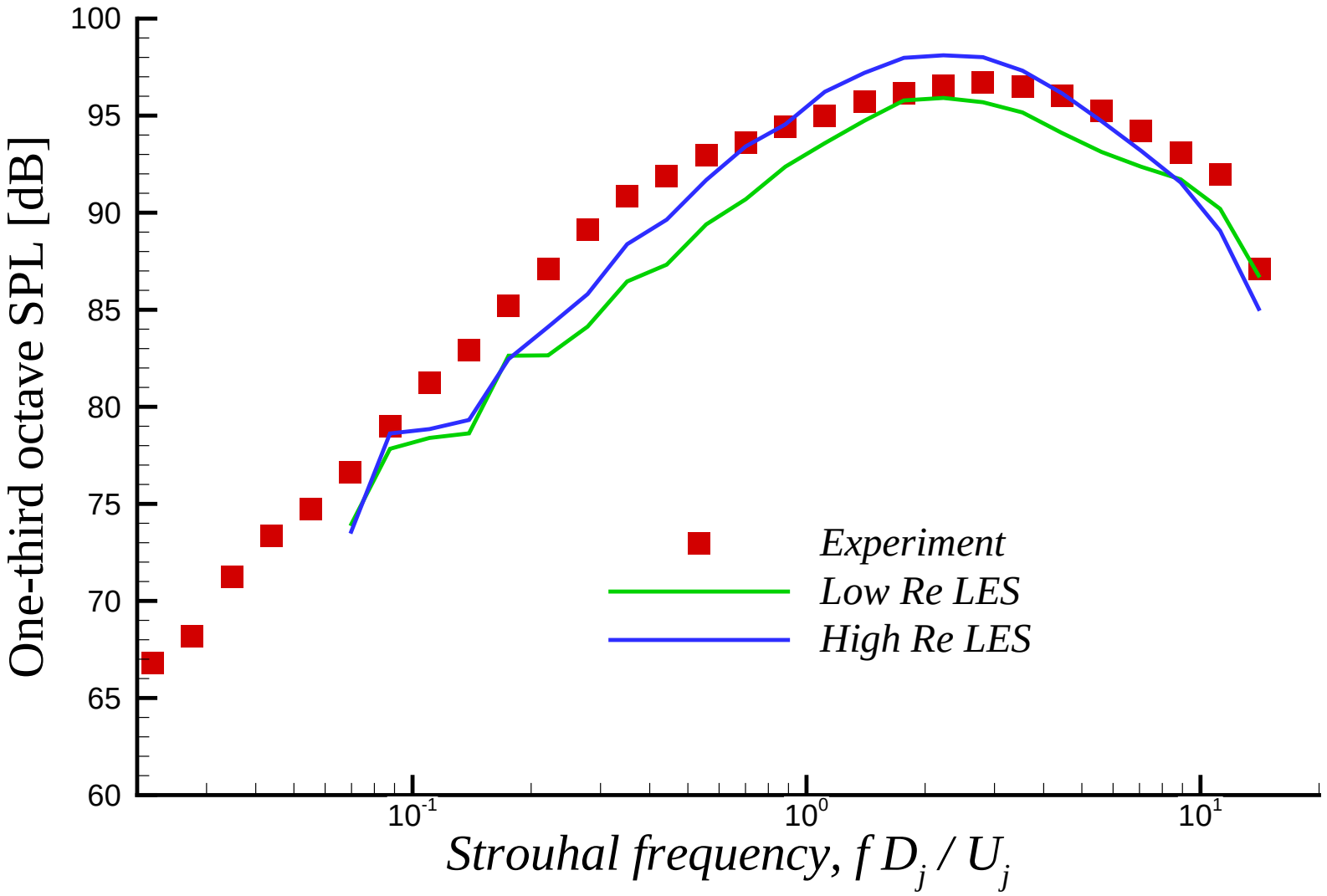

Micro-Actuators for Active Flow Control

- This project is concerned with the development of resonance-enhanced micro-actuators
- These micro-actuators generate pulsed micro-jets for active flow and noise control applications
- Example application: Jet noise control

Micro-Actuators for Active Flow Control

- **Resonance-enhanced micro-actuators provide a capability to adjust micro-jet pulse frequency & amplitude for control application of interest**

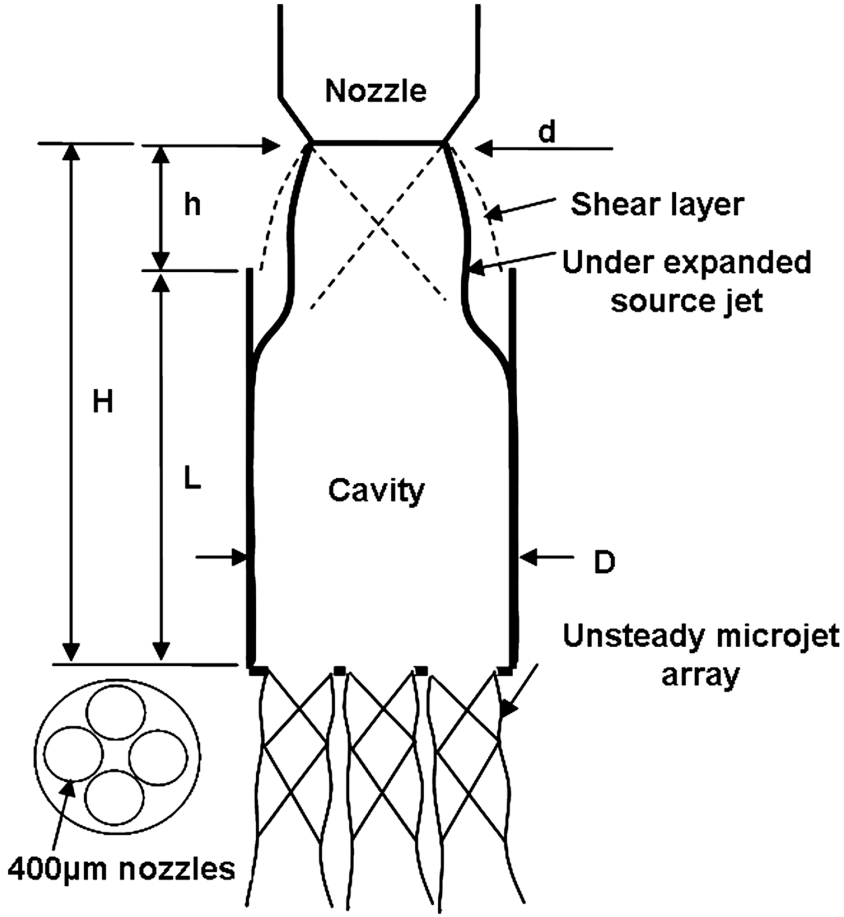

Micro-Actuator Resonance Frequency

- Simulations reveal the complex details of the "aero-acoustic" resonance, which involves a periodic filling and discharging of actuator cavity volume
- Actuator resonance frequency is determined by how quickly the actuator cavity fills and discharges
- Resonance frequency is dependent on actuator dimensions as well as incoming source jet conditions
- Micro-jet pulse frequency is the same as the actuator resonance frequency

Single-Orifice Micro-Actuator Chosen for Simulation

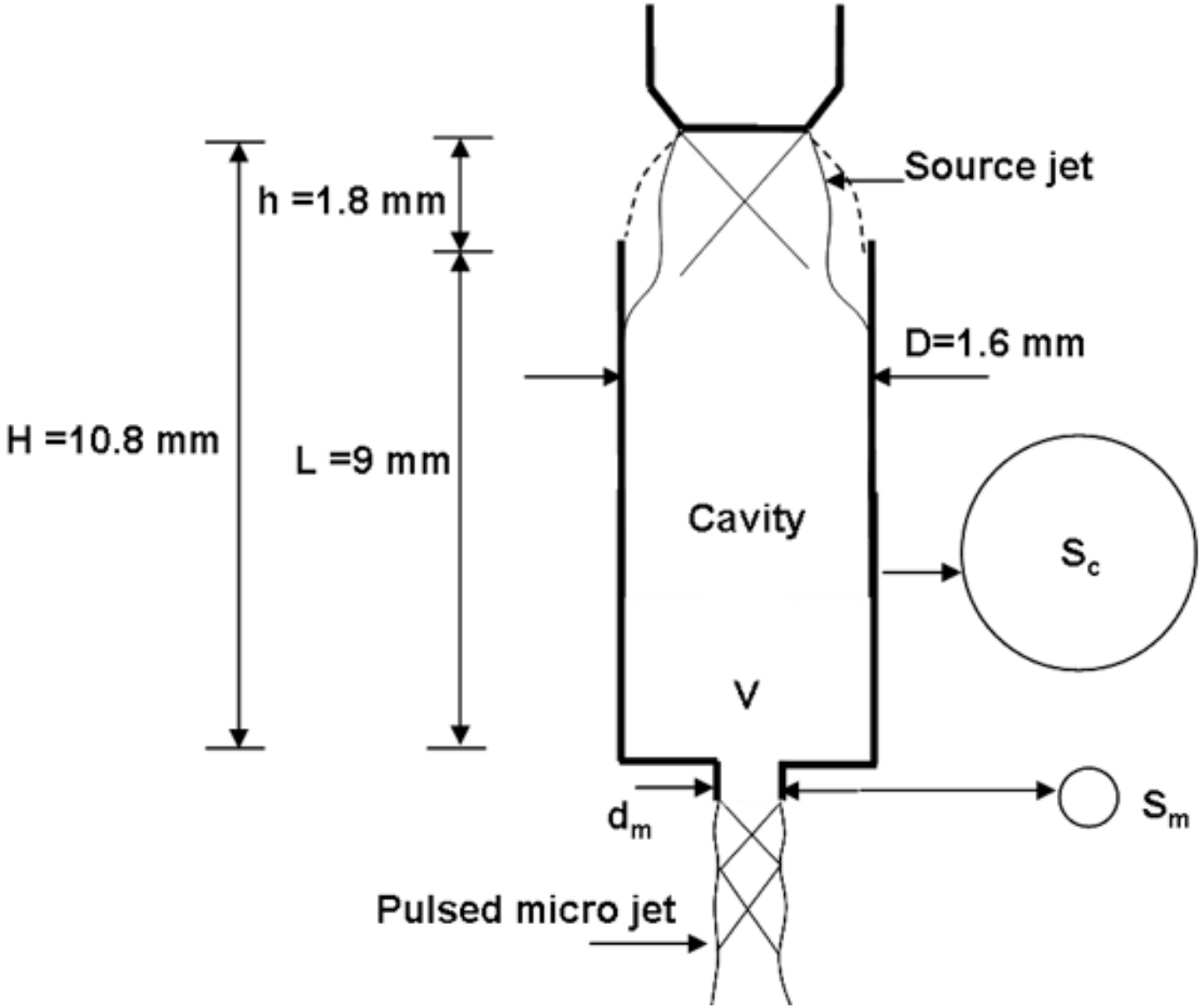

Experimental Spectra of Micro-Jet Generated by Single-Orifice Micro-Actuator

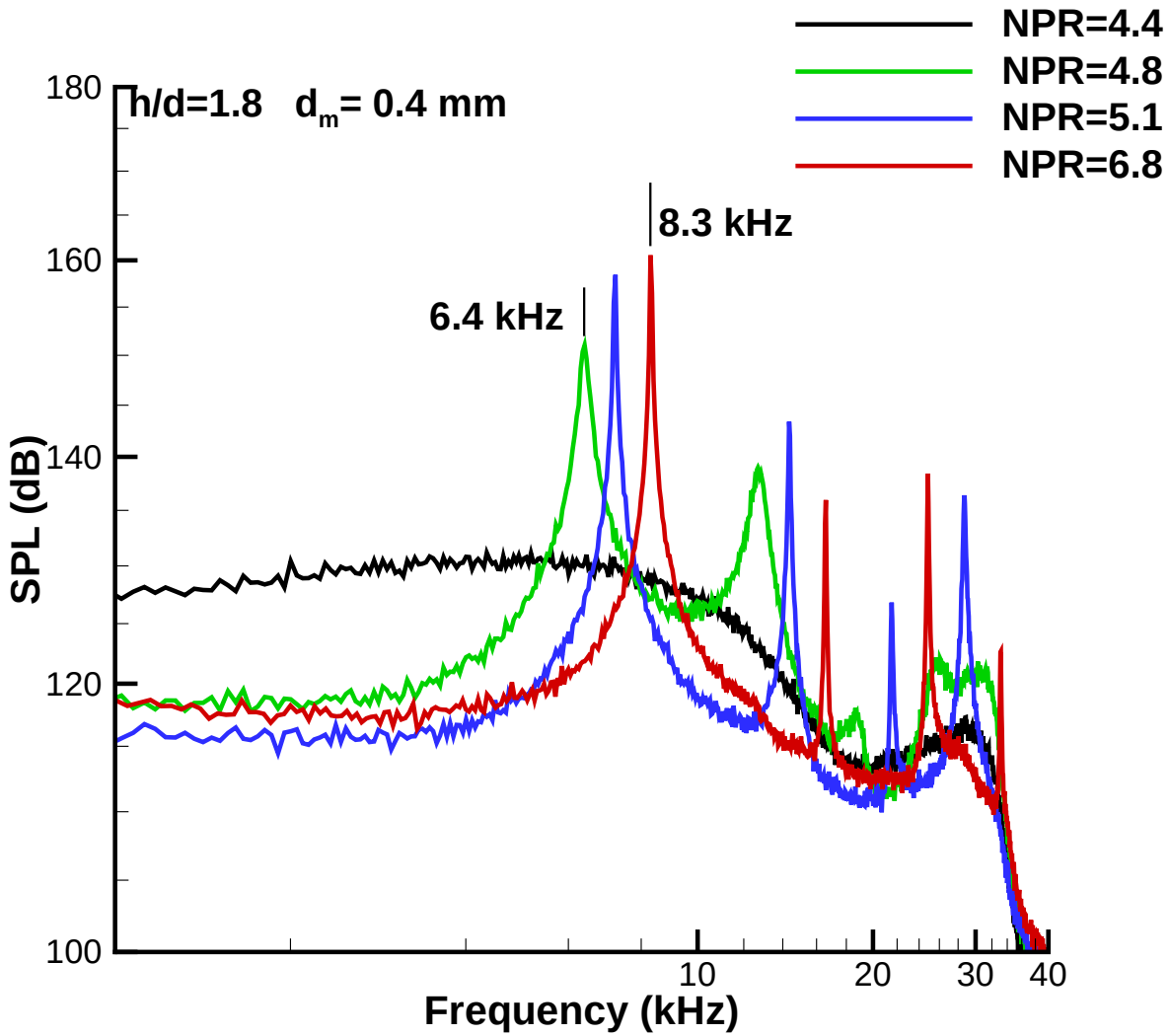

Single-Orifice Micro-Actuator Simulation

- **Length scale = source jet nozzle inner diameter,** $d = 1$ **millimeter**
- **Velocity scale = source jet exit speed** ≈ 343 **meters/second**
- **Reynolds number,** $Re_d = U_j d/\nu_j \approx 37,000$
- **Source jet nozzle pressure ratio,** $\mathbf{NPR} = 6.8$
- **Peak Mach number in actuator flowfield** ≈ 1.8
- **Highly compressible and unsteady micro-scale flow at relatively low Reynolds number**
- **Fully 3-D large eddy simulation (LES) using** 92 **million grid points total**

Simulation Animations

- **Actuator simulation animations and comparison with experimental measurements are available at the following link: http://www.math.fsu.edu/~auzun/SingleOrificeActuator/**

Qualitative Comparison with Experiment

- We make a qualitative comparison between simulation predicted flowfield and experimental micro-schlieren measurements over one cavity fill-and-discharge cycle
- One periodic cycle (which covers 360 degrees) is divided into 12 equally spaced snapshots
- The phase difference between two successive snapshots is 30 degrees
- In the experiment, the cavity is not transparent and thus the cavity flow cannot be visualized
- We omit the cavity region in the comparison

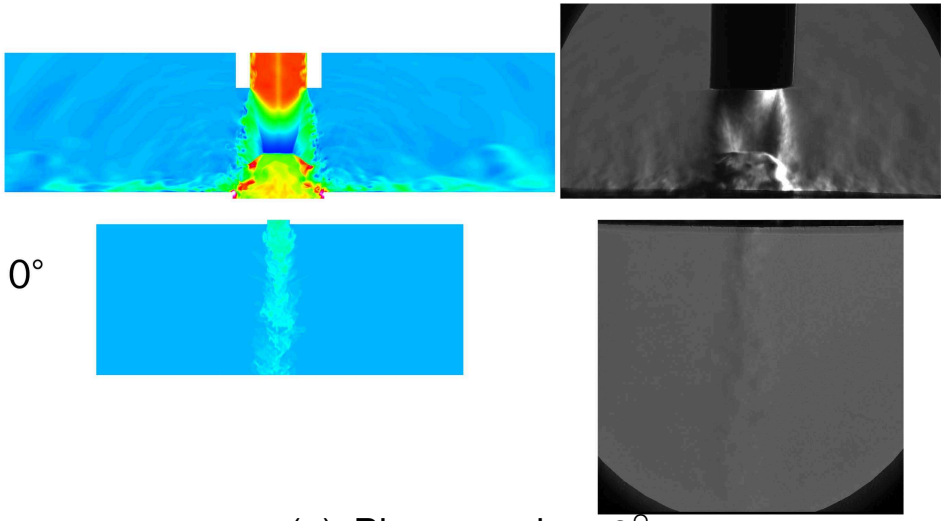

(a) Phase angle = 0°

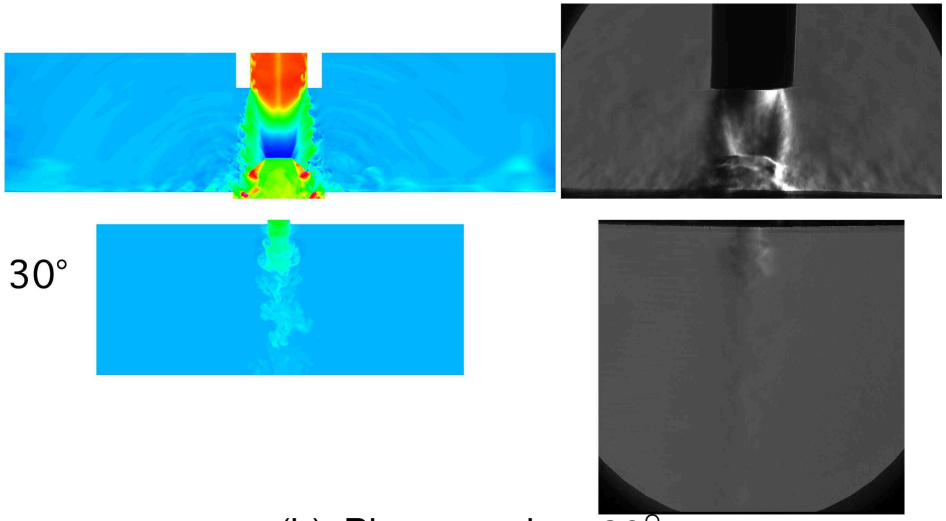

(b) Phase angle = 30°

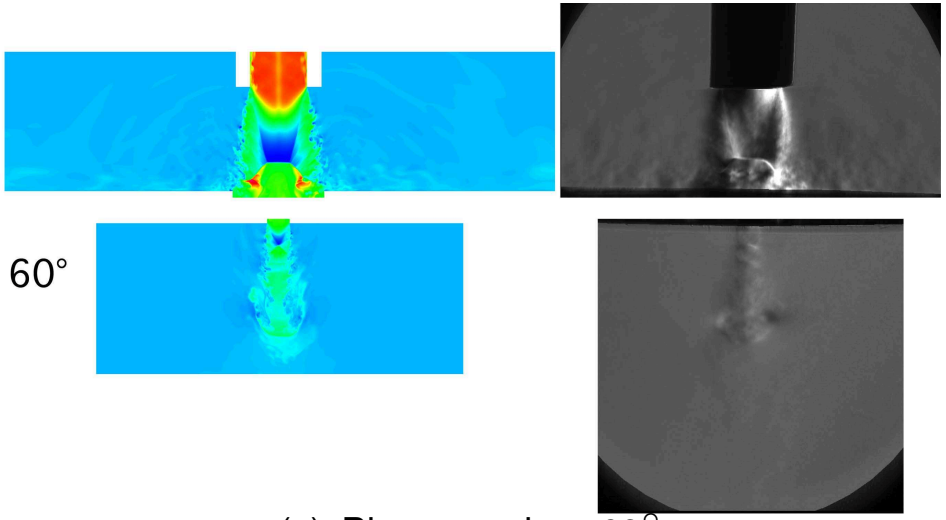

(c) Phase angle = 60°

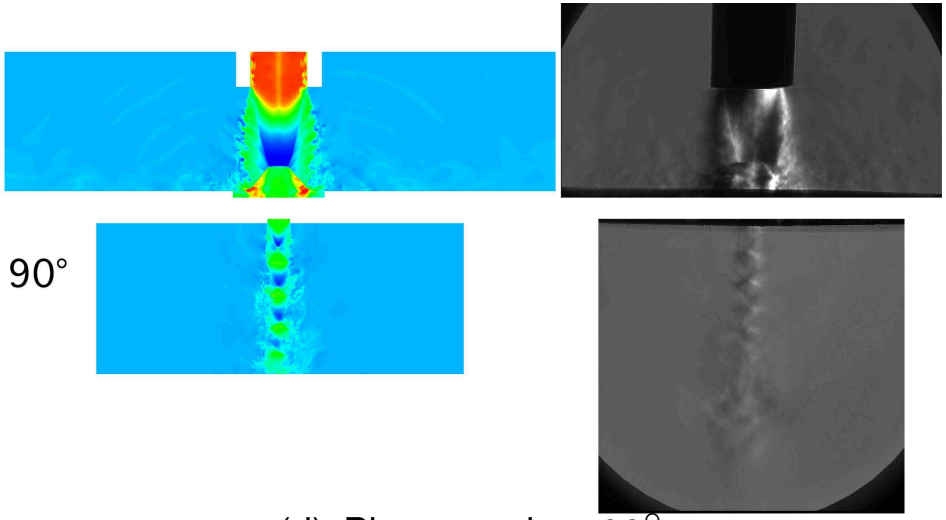

(d) Phase angle = 90°

Color map represents normalized density, $\rho/\rho_{\mathbf{ambient}}$

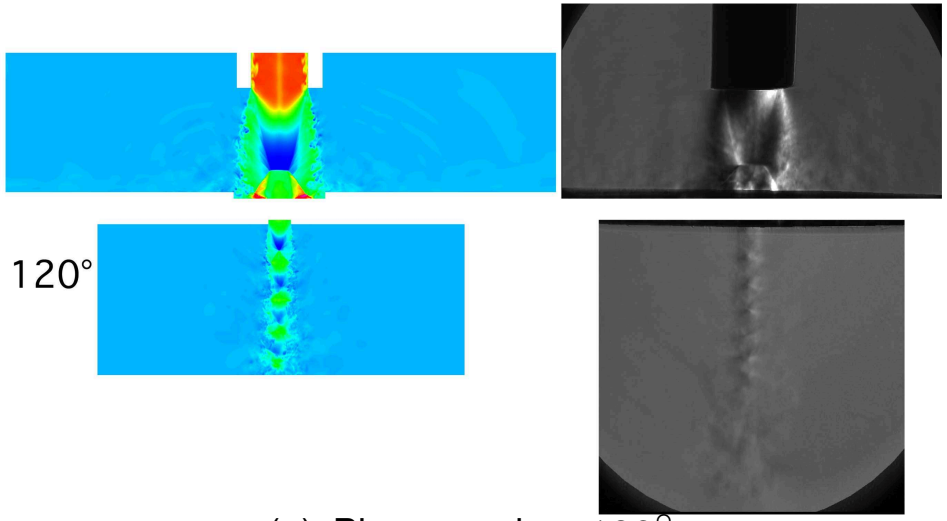

(a) Phase angle = 120°

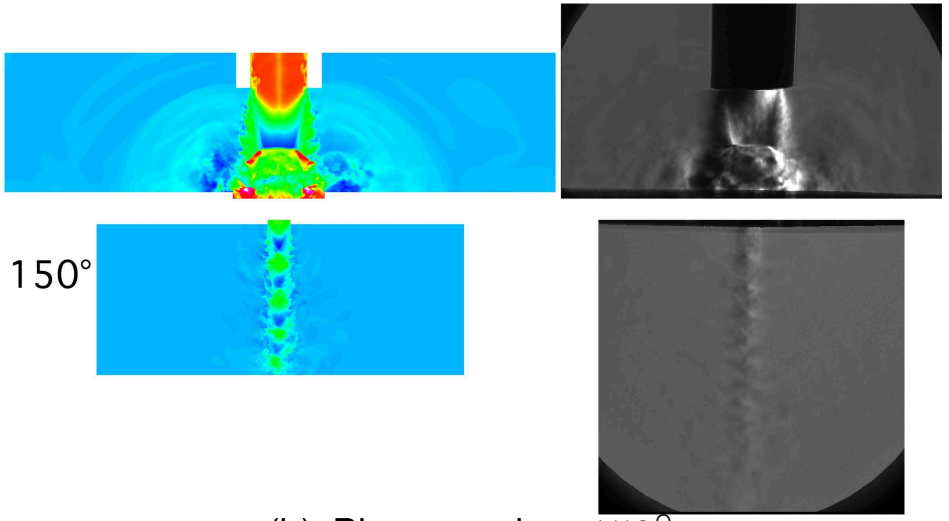

(b) Phase angle = 150°

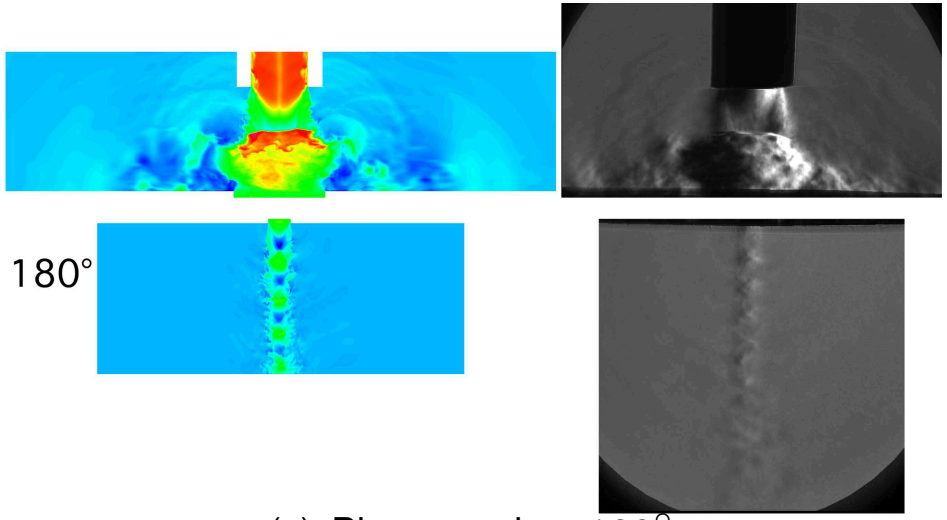

(c) Phase angle = 180°

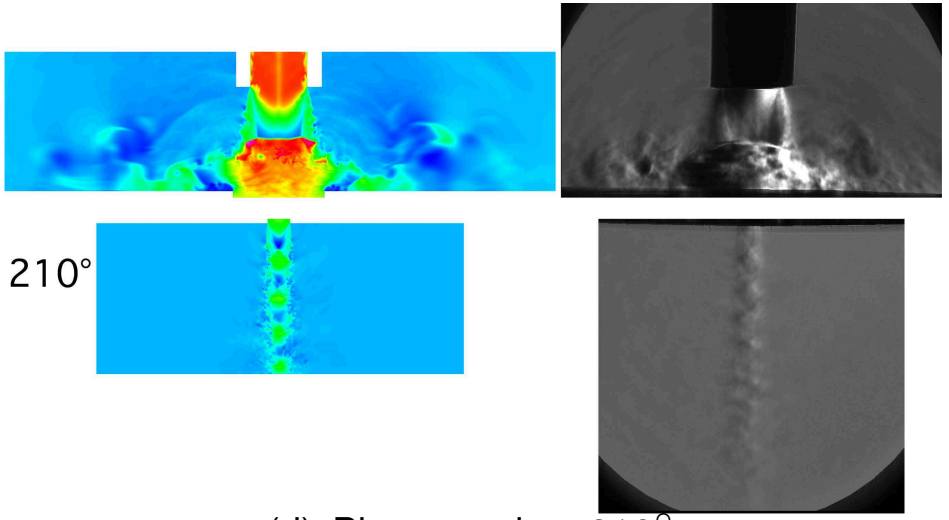

(d) Phase angle = 210°

Color map represents normalized density, $\rho/\rho_{\mathbf{ambient}}$

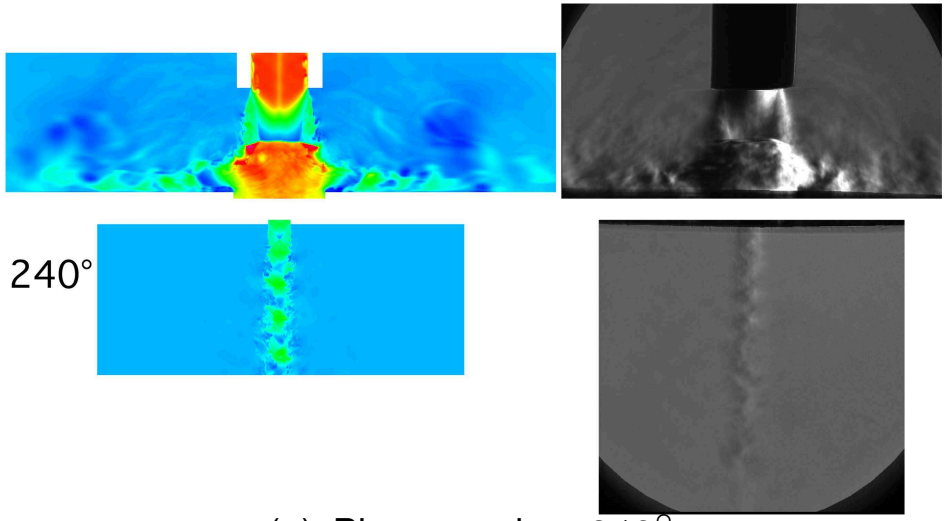

(a) Phase angle = 240°

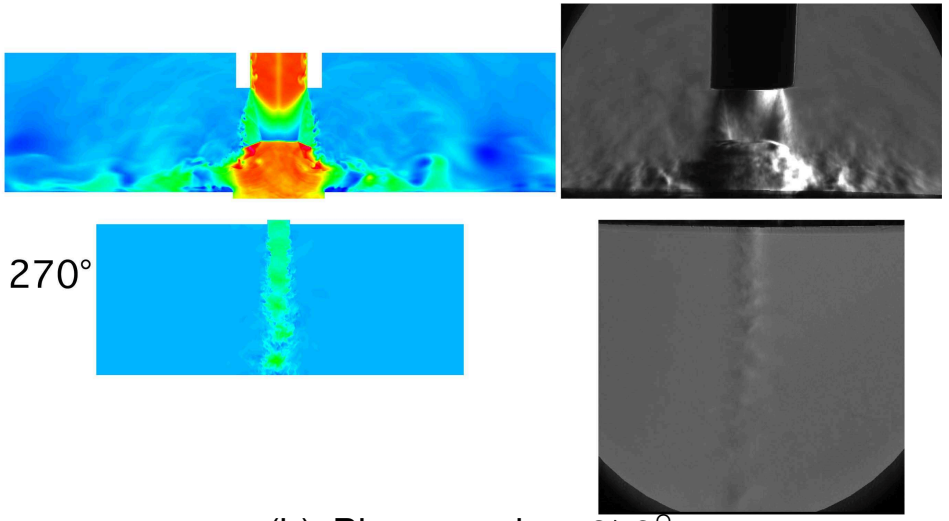

(b) Phase angle = 270°

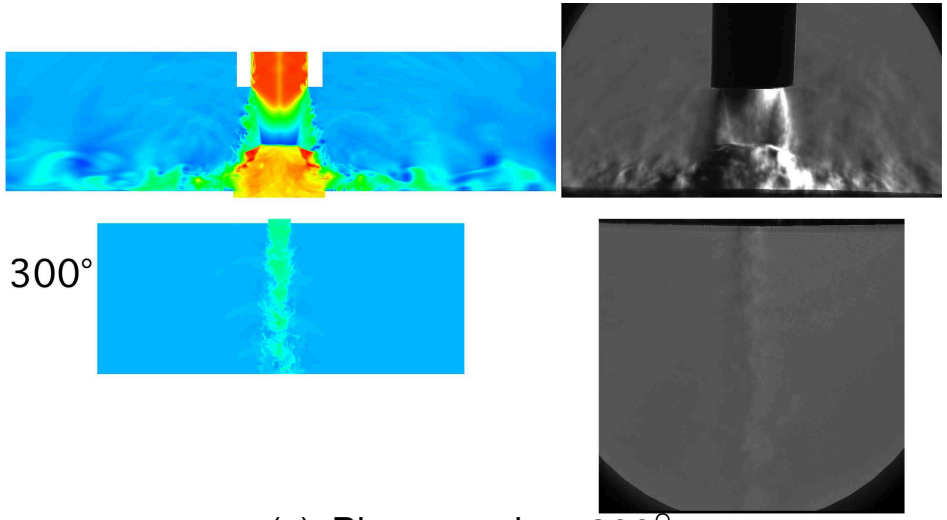

(c) Phase angle = 300°

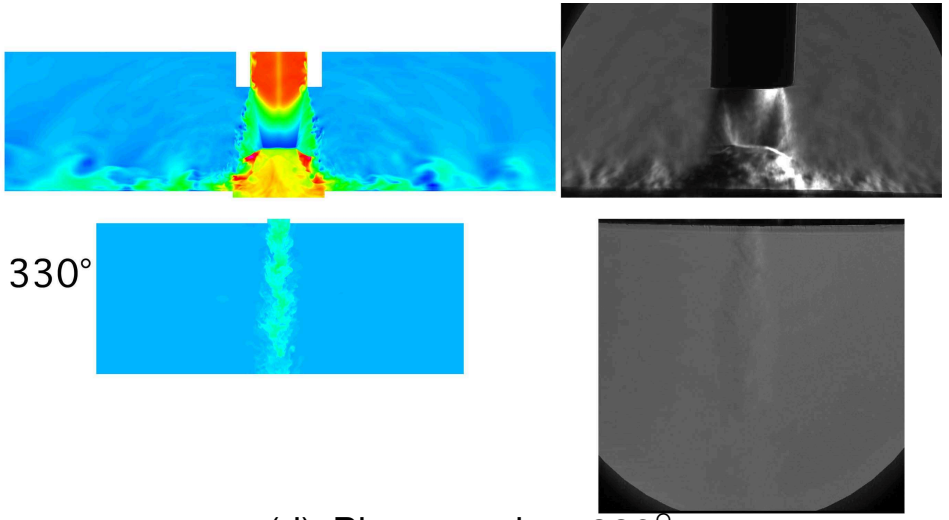

(d) Phase angle = 330°

Color map represents normalized density, $\rho/\rho_{\mathbf{ambient}}$

Supersonic Impinging Jets

- **An important problem for short take-off and vertical landing (STOVL) aircraft**

Supersonic Impinging Jets

- High-speed jet impingement on landing surface leads to many adverse effects such as:
  - High levels of unsteady pressure loads on landing surface and nearby structures
  - Significantly higher noise levels than conventional take-off aircraft
  - Aircraft lift loss during hover
  - Erosion of landing surface due to high jet exhaust temperature
- Resonance dominated flowfield that is governed by a well-known feedback loop

Schematic of Feedback Loop

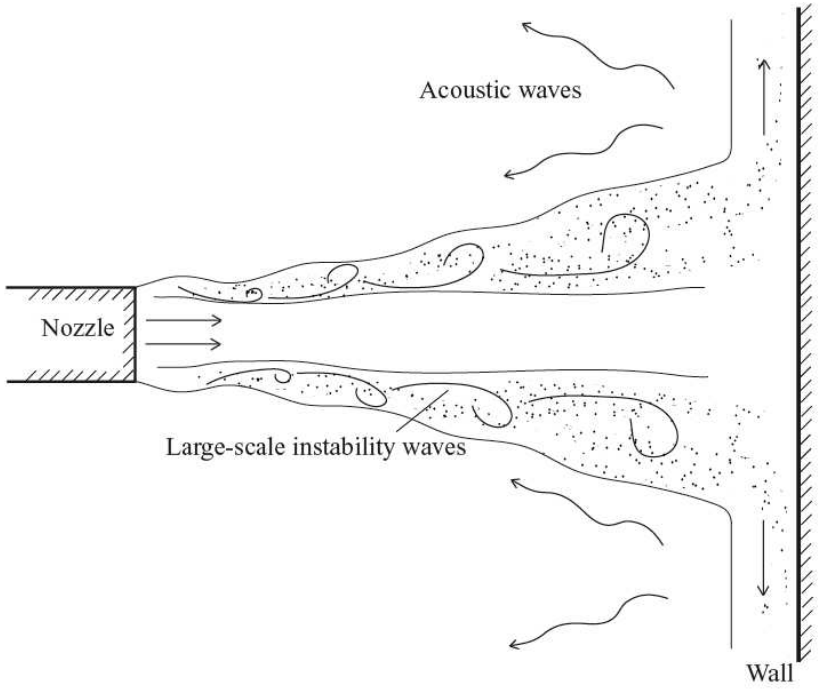

- Large scale vortical structures generate strong pressure fluctuations upon impingement
- Pressure fluctuations propagate upstream, exciting instabilities in the jet shear layer
- Excited instabilities give rise to the formation new vortical structures

Schematic of Experimental Setup

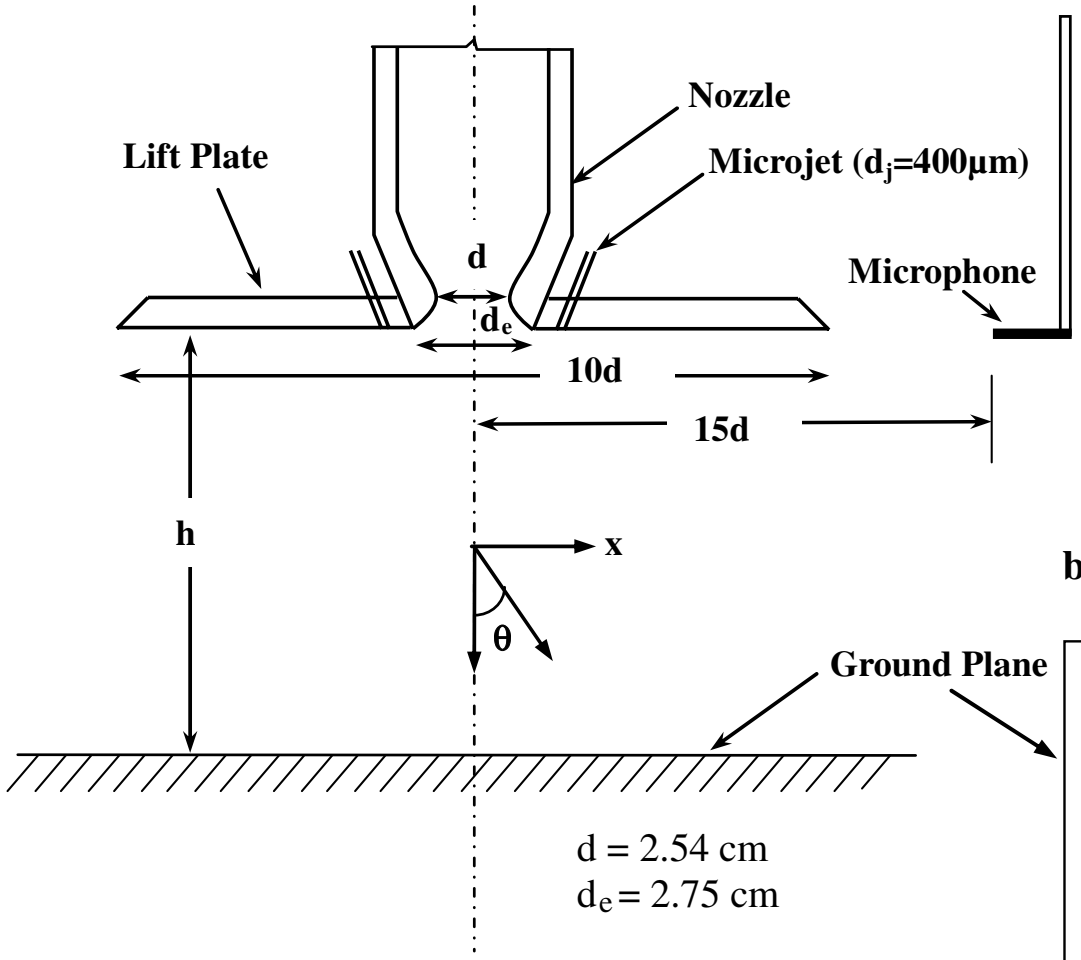

a)

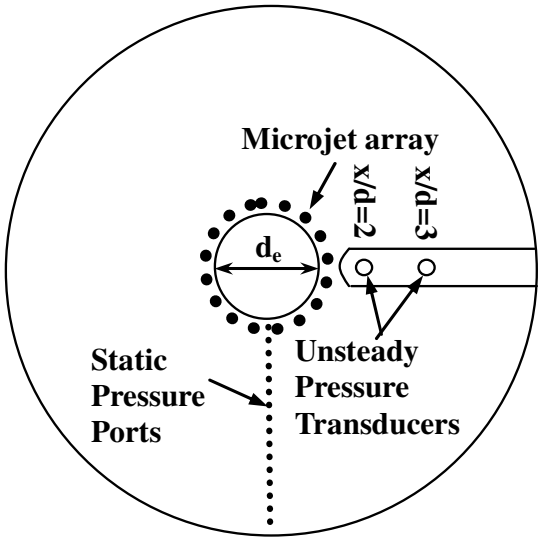

b)

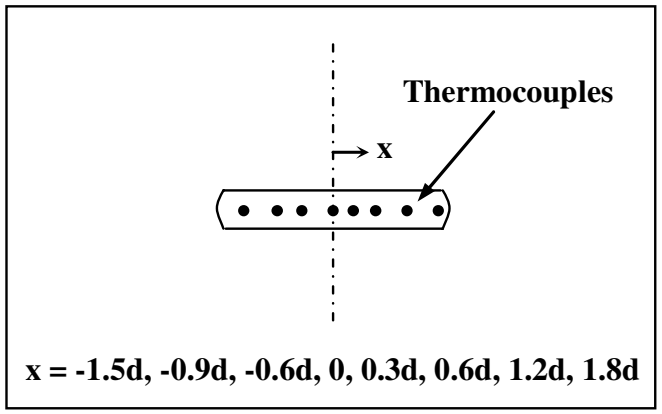

c)

Near-Ideally Expanded Mach 1.5 Uncontrolled Impinging Jet Simulations

- **Near-ideally expanded isothermal and heated jet simulations matching experimental cases**
- **Reynolds number range** $\approx 0.9 \times 10^6$ **to** 1.3×10^6
- **Ratio of jet impingement distance to nozzle throat diameter,** $h/d = 5$
- **Experimental setup is duplicated in the simulations**
- **Laminar nozzle inflow conditions**
- **Fully 3-D LES using** 200 **million grid points**

Isothermal Mach 1.5 Jet Mean Flow Streamlines

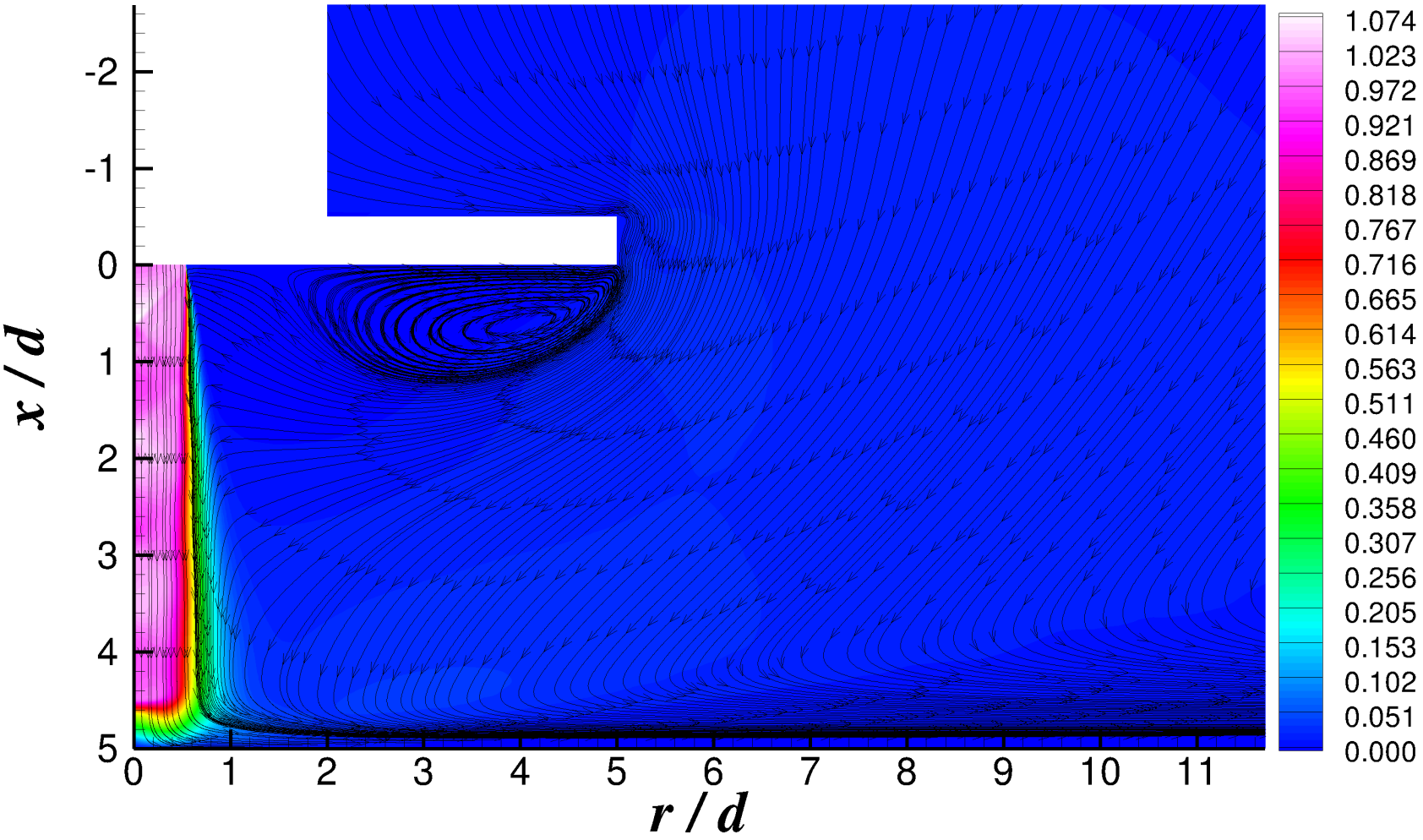

Temperature Contours of Heated Mach 1.5 Impinging Jet

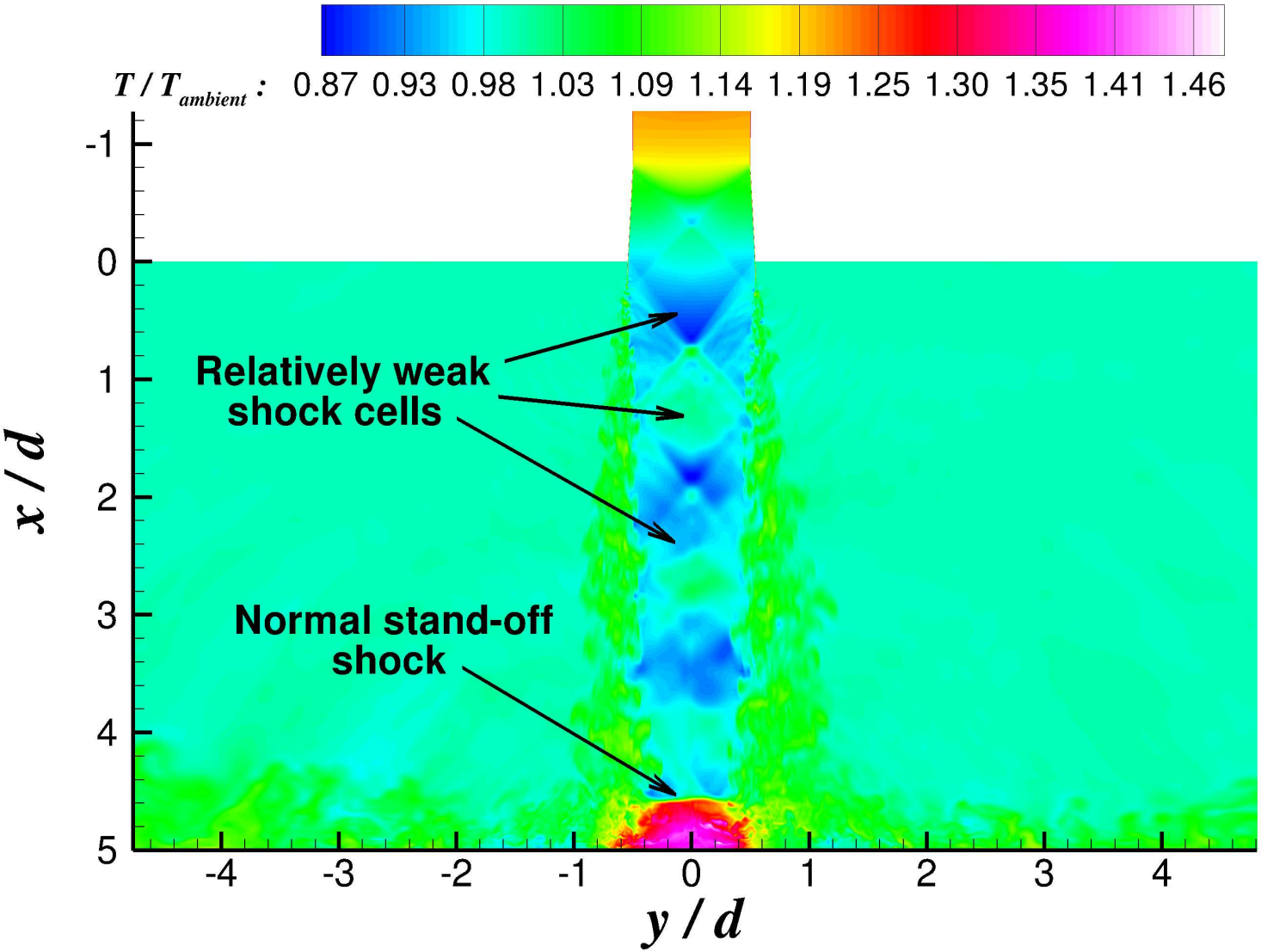

Heated Mach 1.5 Jet Normalized Mean Axial Velocity (U/U_j) Contours

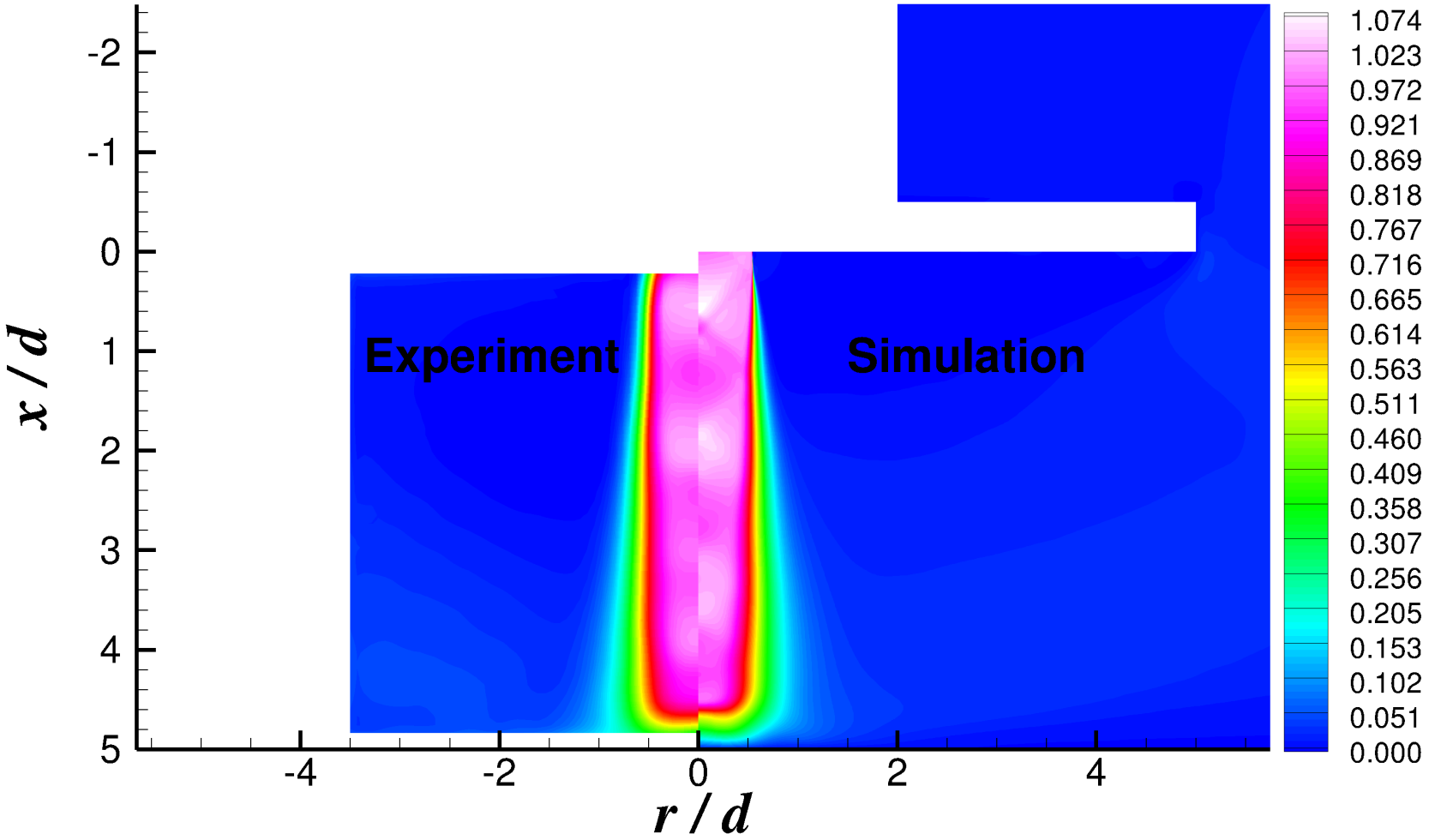

Comparison of Normalized Mean Axial Velocity Profiles for Heated Mach 1.5 Jet

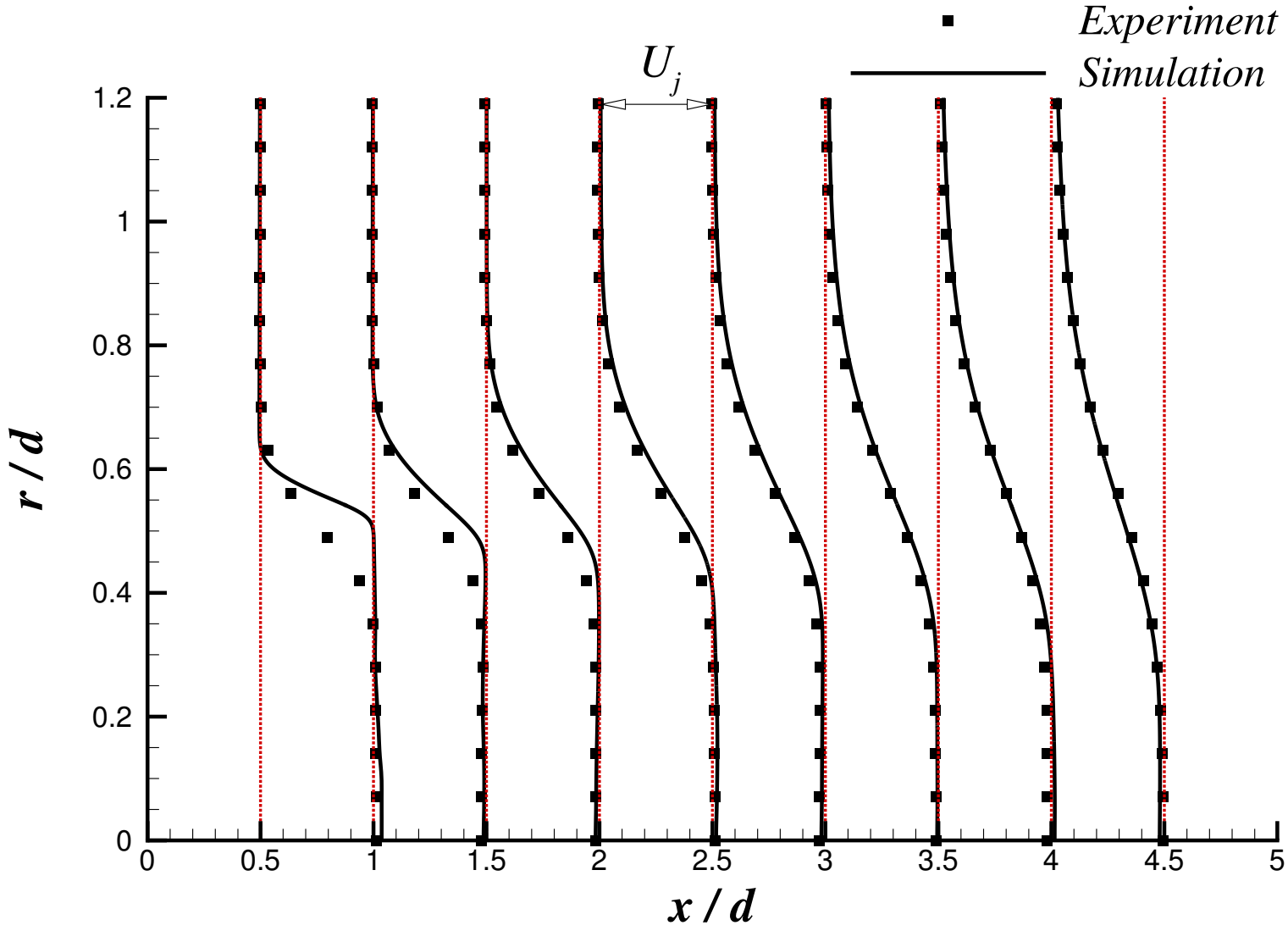

Comparison of Microphone Noise Spectra for Heated Mach 1.5 Jet

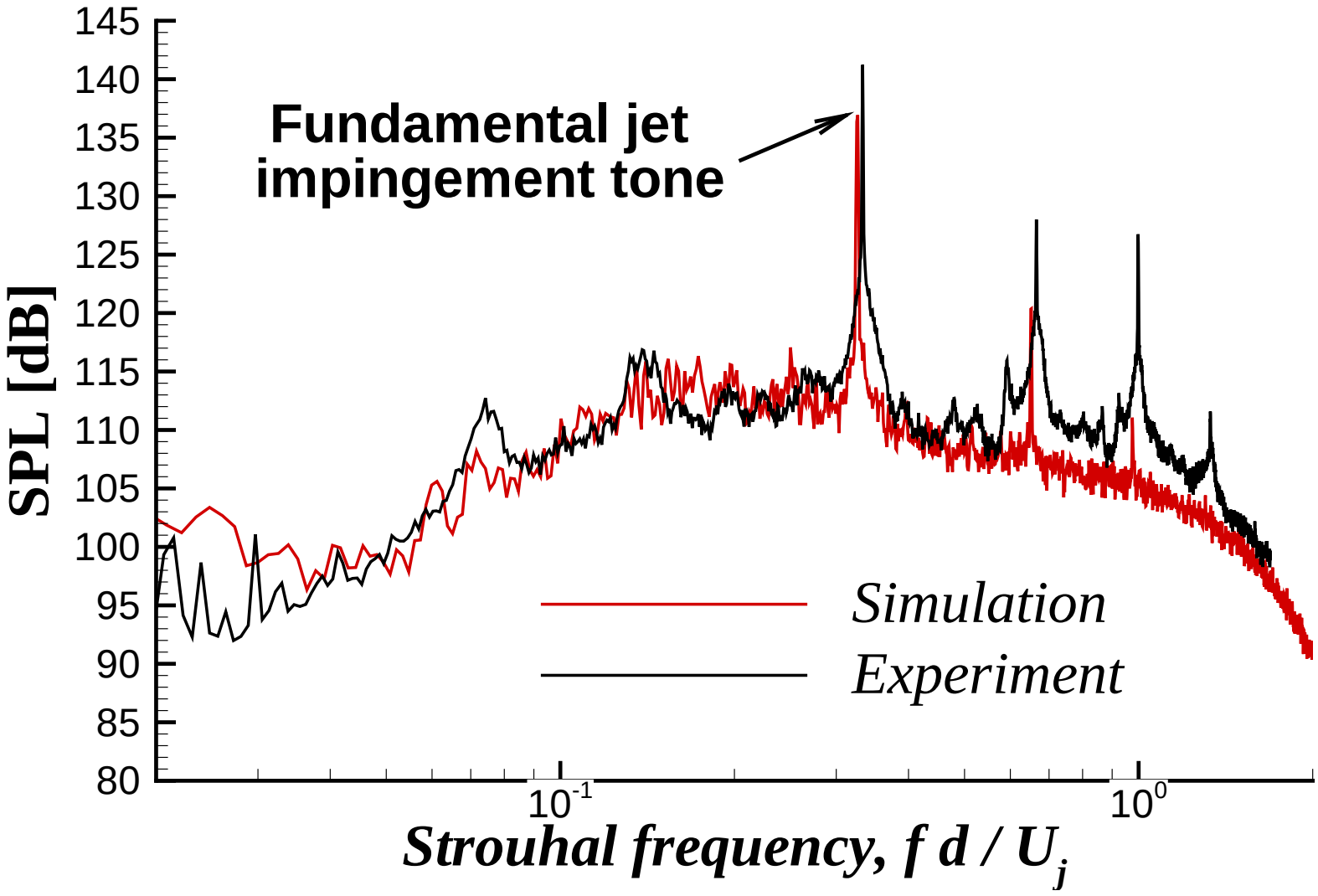

Identification of Coherent Structures

- **Dynamic mode decomposition (DMD) has been utilized to identify the coherent structures that are responsible for intense tonal generation in supersonic impinging jets**
- **DMD (Schmid, JFM 2010) is a technique that allows the extraction of dynamically relevant flow features from a uniformly sampled data sequence, available from the simulations**
- **We utilize a total of nearly 800 flowfield snapshots with a uniform $\Delta t = 0.25 d/U_j$ for DMD analysis**

Coherent Structures Identified by DMD

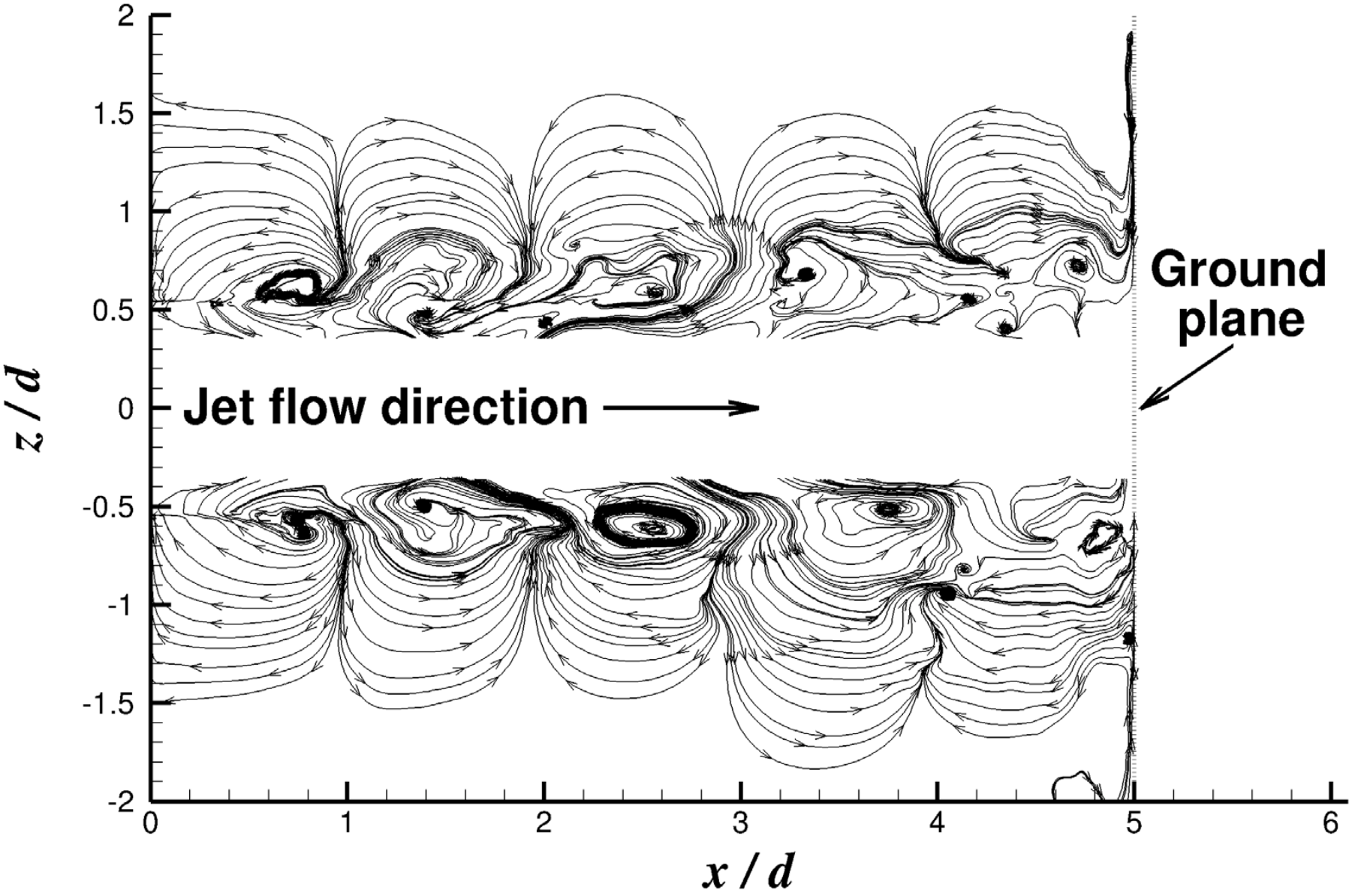

Pressure Disturbance Iso-Surfaces Associated with Vortex Rings

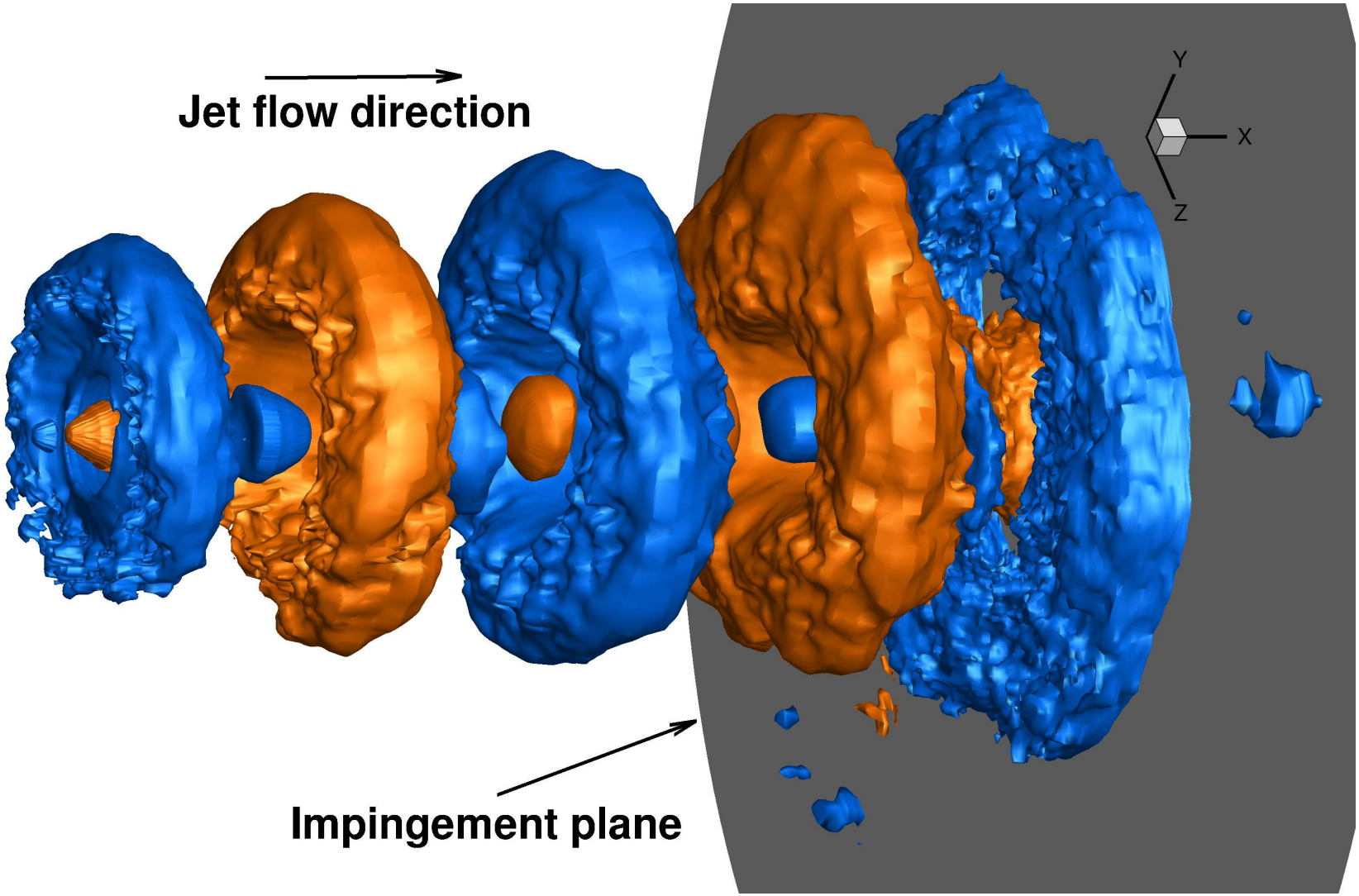

Current Applications of Simulation Methodology

Transition Delay on Swept Wings via Spanwise-Periodic Roughness Elements

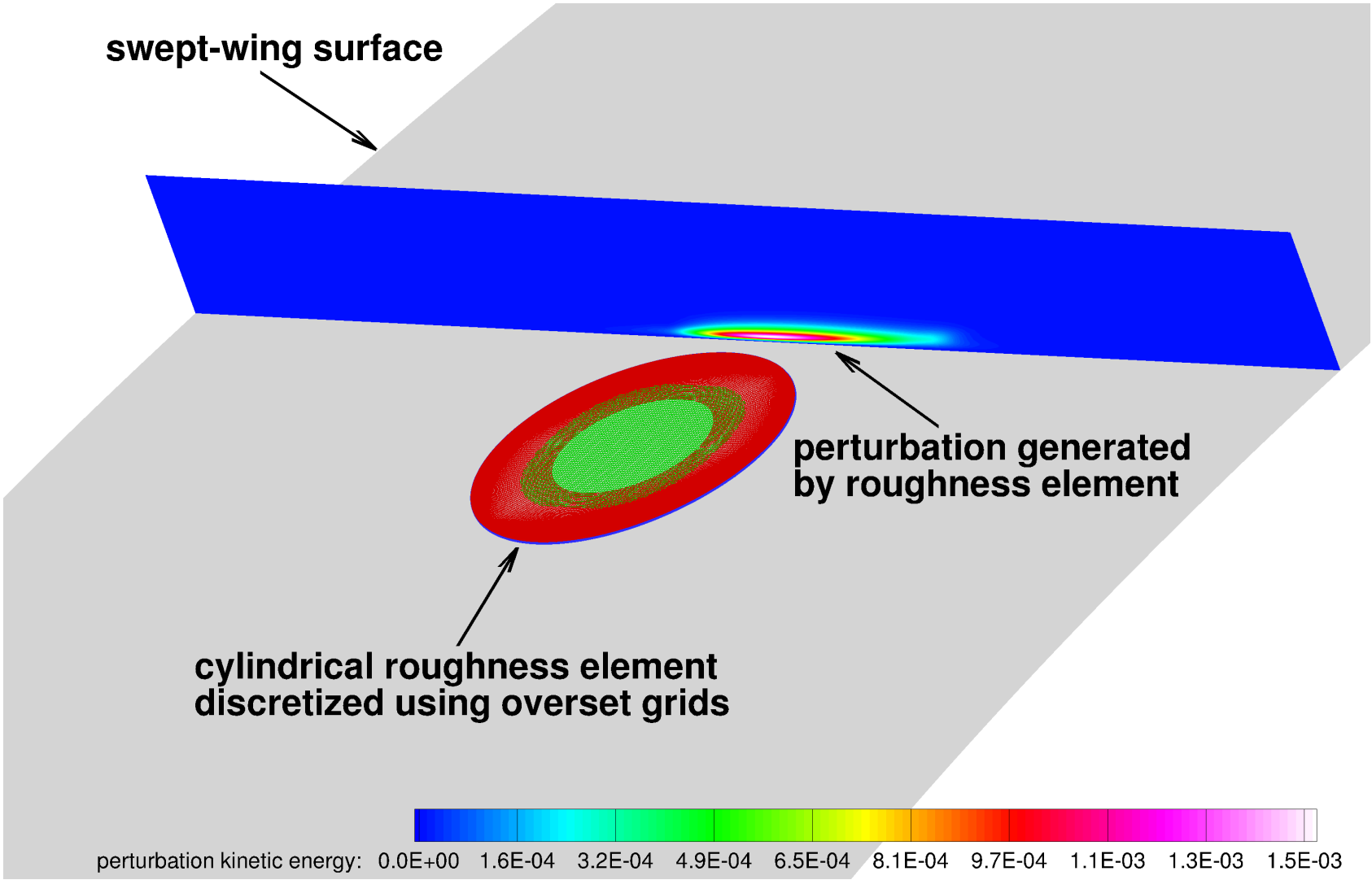

Flow Separation on Wall-Mounted Hump

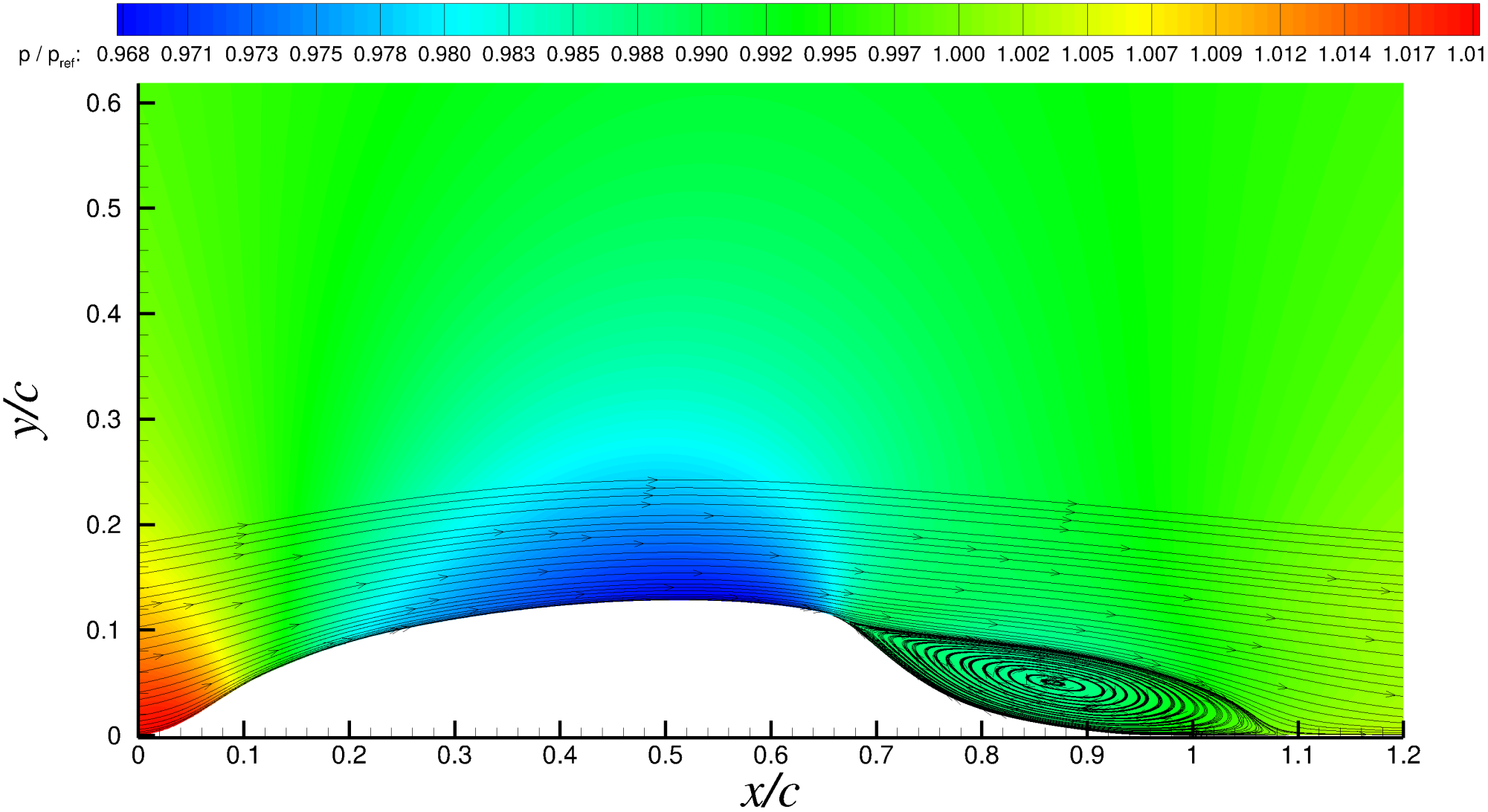

Summary and Outlook

- High-order, high-fidelity simulation methodology applicable to practical high-speed flows
- Good overall agreement between experiments and simulations has been observed
- We are currently using this methodology to study problems of interest to NASA
- We plan to port this capability on GPUs & peta-scale machines and perform well-resolved simulations of complex high Reynolds number flows in near future